Design and Construction Elements for Scintillating Fibre Tracking Detectors

By
Jason Ray Sharpe

A Thesis Submitted to Saint Mary's University, Halifax, Nova Scotia,
in Partial Fulfillment of the Requirements for the
Degree of Master of Science in Applied Science

April, 2012, Halifax Nova Scotia

Approved: Dr. Adam J. Sarty
Supervisor
Department of Astronomy and Physics

Approved: Dr. Robert D. Singer
Supervisory Committee Member
Department of Chemistry

Approved: Dr. Mahbub A. Khandaker
Supervisory Committee Member
Department of Physics
Norfolk State University

Approved: Dr. David L. Hornidge
External Examiner
Department of Physics
Mount Allison University

Approved: Dr. Hai Wang
Graduate Studies Representative

Date: April 17th, 2012

Library and Archives Canada

Published Heritage Branch

395 Wellington Street
Ottawa ON K1A 0N4
Canada

Bibliothèque et Archives Canada

Direction du Patrimoine de l'édition

395, rue Wellington
Ottawa ON K1A 0N4
Canada

Your file Votre référence
ISBN: 978-0-494-87686-2

Our file Notre référence
ISBN: 978-0-494-87686-2

Design and Construction Elements for Scintillating Fibre Tracking Detectors

By Jason Ray Sharpe

Abstract: In many nuclear and particle physics experiments, it is necessary to ascertain precise information about a particle's trajectory, or its position at specific locations (as a means for then determining angle or momentum). A common way to determine this information is by using a scintillating fibre tracker, a device that relies on scintillation light from ionizing charged particles (such as electrons or protons) within scintillating fibres, and guiding the produced scintillation light through standard fibre optics to determine which scintillating fibre detected the particle. This thesis discusses, and presents results for technical issues associated with designing and constructing such a detector: (1) adjacent scintillating fibre-to-fibre cross-talk, and (2) the effect on light transmission of the combination of different fibre-end finishes and clear-to-scintillating fibre optical couplants. These results will be directly incorporated into the construction of a scintillating fibre coordinate detector to be built for future experiments at Jefferson Lab's Hall A in Newport News, VA, USA.

April 17th, 2012

Contents

List of Figures

List of Tables

Acknowledgements

I would like to sincerely thank my supervisor, Dr. Adam J. Sarty (Saint Mary's University - Dept. of Astronomy and Physics), who has been my academic mentor for nearly three years now. He has been patient with me, calm, and helping when I needed it. He showed me how to relax, take a breath and approach problems from a new angle when I was struggling. He also helped restore my intellectual confidence that has been missing for many years. I hope to be able to work with him again in the future.

I would also like to offer my thanks to my parents, Clinton and Anna Sharpe, who have always been there for me as I worked to achieve my goals. They have always provided support when it was needed, and a pat on the back when it was deserved. I am very glad I'm able to make them proud.

I would like to thank my committee members, Dr. Mahbub A. Khandaker (Norfolk State University - Dept. of Physics) and Dr. Robert D. Singer (Saint Mary's University - Dept. of Chemistry), as well as my external reviser, Dr. David L. Hornidge (Mount Allison University - Dept. of Physics) for guiding me through this degree, and helping me complete my thesis, on time.

I also offer many thanks to Dr. Michael Dunlavy (Saint Mary's University - Dept. of Physics) and my friend Jeffrey Woodacre, for providing me with hours of their time to help me come up with new ideas, provide technical support, aid me with computer programming and for simply offering outside views on such an involved

topic. Their help has been invaluable to the completion of this degree.

I would also like to thank my uncle, Andrew G. Sharpe. for helping me with my thesis corrections. and providing academic guidance, from before I started university, until now. Without his counsel, my future choices would be much less clear.

Finally, I would like to point out that thanking everyone that has aided me in achieving this Master of Science degree is an impossible task. Everyone from my family, significant other, friends, and acquaintances have made an impact. It is also hard to measure the importance of even a simple comment or sentence on the outcome of a scientific project. I thank all of you for your help over these last two years.

-Jason R. Sharpe

Chapter 1

Introduction

1.1 General Goal of Thesis

The goal of this thesis is to investigate common design characteristics of scintillating fibre trackers. In particular, to study adjacent fibre cross-talk and fibre-to-fibre light transmission.

1.2 Scintillating Fibre Trackers

A scintillating fibre tracker (SFT) is an ionizing particle detector that is able to provide position and trajectory information of ionizing particles that pass through it. A passing particle excites a scintillating fibre which emits light via scintillation. The scintillation light travels down the scintillating fibre and passes into a light guide (standard fibre optic as used in telecommunication). The light is then carried to a light collection device to be converted into an electrical signal. An example of a basic x and

y plane SFT is shown in Figure 1.1. These fibre trackers started being conceived and built in the 1980's by a number of different research groups [1–6] and quickly became used as position sensitive calorimeters [7] and more accurate hodoscopes [8, 9]. By the mid 1990's SFTs were being used in particle accelerators around the world [10].

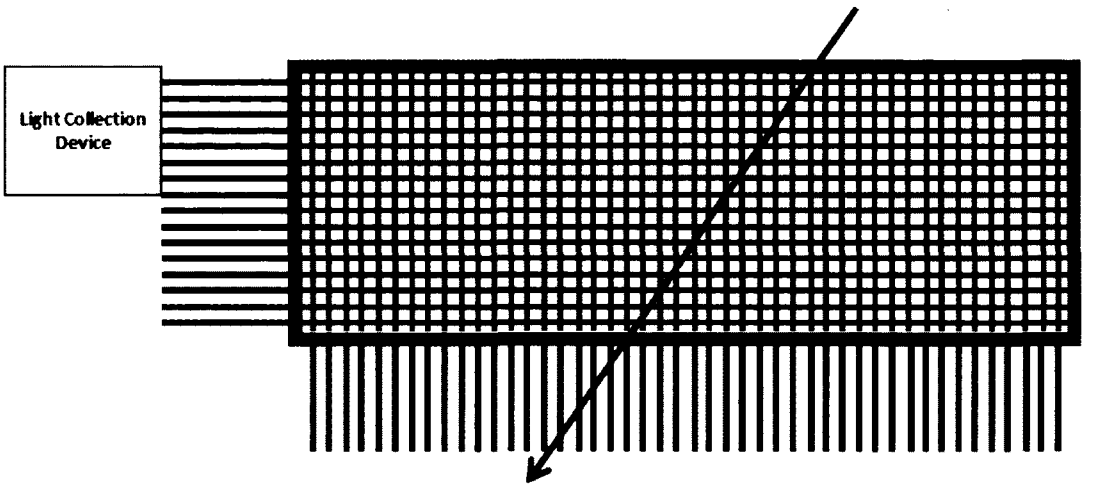

Figure 1.1: Ionizing particles pass through the SFT (in reality, the spacing between the fibres can be very small). An ionizing particle deposits a small amount of energy into a scintillating fibre, releasing photons. The photons travel down the scintillating fibre, into a light guide, then into a light collection device. The activation of specific light collection devices (or particular pixels on one light collection device) will thus reveal the position of the passing particle.

These detectors are used throughout the science community for a number of different applications, from biology to astrophysics. For instance, SFTs have been adapted for Restriction Landmark Genomic Scanning Technology, a rapid method for the genetic analysis of many organisms [11]. Additionally, scintillating fibres trackers

have been used for DNA sequencing [12, 13]. Furthermore, atmospheric physicists have used SFTs to determine the flux of incoming radiation in the upper atmosphere by placing trackers on hot air balloons [14]. SFTs can also be used to determine the luminosity of the 7 TeV particle beam in the Large Hadron Collider (LHC) for the Toroidal LHC Apparatus (ATLAS) experiment [15, 16].

Equally important are Positron Emission Tomography (PET) scans, where patients are injected with a radioactive tracer. Tracers are absorbed by certain parts of the body and emit positrons that exit the patients and activate scintillating fibres in a surrounding PET module. The result is a 4 dimensional (including time) view of processes occurring in regions of the body under study. SFTs are able to detect a large variety of particles, with a range of energies, making it possible to use different tracers to study many biological processes in the body. The spatial resolution of a PET camera has been studied and found to be 2.0 mm [17].

Finally, SFTs are most frequently used in nuclear and particle physics experiments, since they provide excellent position and temporal resolution in high rate experiments [18].

1.3 Fundamentals of Scintillation

The first scintillation counter was built in 1903 by Sir William Crookes [19, 20]. The device consisted of a ZnS screen which produced weak scintillation when struck by α-particles [21]. A microscope was used to view the scintillation effects and a maximum counting rate of about one particle second was achieved. The invention of this scintillation counter later led to Rutherford's discovery of the atomic nucleus [19].

Scintillation falls into a sub-category of fluorescence, which refers to a mechanism that releases energy in the form of light after the absorption of energy through some other means. There are three types of fluorescence: prompt fluorescence, delayed fluorescence and phosphorescence. Prompt and delayed fluorescence have the same light spectrum, whereas phosphorescence is typically very slow and has a light spectrum shifted to longer wavelengths [20].

Scintillation refers to prompt fluorescence caused by the passage of ionizing radiation. The prompt time scale is on the order of nanoseconds, which is an important feature for particle physics experiments wherein detectors are subjected to very high rates, on the order of a $10^8 - 10^9$ events per second [20].

An important characteristic of a scintillating material is its scintillation efficiency. This is defined as the fraction of a passing particle's deposited energy in the scintillating material that appears as visible radiation [22]. A higher scintillation efficiency always is preferred.

Scintillation occurs in two different categories of materials: organic and inorganic scintillators. The mechanism is quite different between the two. With inorganic scintillating materials, individual molecules are responsible for the scintillation process. In contrast, in organic materials entire chains of molecules are excited. With inorganics, scintillation efficiency is high but they are extremely slow compared to organics, where the scintillation efficiency is smaller [22].

For organic scintillators, the scintillation component of the material has π-electron structures [20,22]. The structures have a number of singlet (S) and triplet (T) states with spins 0 and 1 respectively, where the singlet states are higher in energy.

S_0 is the singlet ground state, where S_1 is the first electronically excited singlet state, etc. These states are separated by 3-4 eV, corresponding to visible light wavelengths, depending on the scintillating material used [20]. Similary, triplet states, T_0, T_1, etc, are present. Each of these states, the singlets and triplets, have a number of vibrational (or thermal) energy levels, which are separated by roughly 0.15 eV [20]. Sometimes these vibrational energy levels are represented by a second subscript as follows: S_{00} or T_{21}, where the first subscript is the electronic state and the second is the corresponding vibrational state.

A passing particle will lose a small amount of energy to many π-electron structures, such that the energy will be used to excite the system up to any one of the states above the S_0 state. Once in the excited state, the system will quickly decay via radiationless internal conversion (also known as internal degradation [20]) to the S_{10} level [20]. Radiationless decay to the S_{10} level occurs extremely quickly ($\sim 10^{-12}$ s), 2-3 orders of magnitude faster than other decay processes (such as the scintillation decay). Once in the S_{10} state, the system can emit visible light and decay to one of the vibrational states of S_0. Sometimes, the S_{10} state will decay to T_{10}, a process called an intersystem crossing [20]. This occurrence accounts for the delayed light release in organic scintillators. Sometimes the T_{10} gains enough vibrational energy to jump back to the S_{10} state, where light is emitted normally. These prompt and delayed light emissions can be characterized by two decay constants, τ_{prompt} and $\tau_{delayed}$. The number of photons emitted from a scintillator is given by [22],

$$n(t) = k(1 - e^{-t/\tau}) \tag{1.1}$$

where $n(t)$ is the number of emitted photons as a function of time, k is the number of electrons capable of causing a light emission and τ is the decay constant. This can be applied to either situation with τ_{prompt} or $\tau_{delayed}$ resulting in:

$$n(t) = k_{prompt}(1 - e^{-t/\tau_{prompt}}) + k_{delayed}(1 - e^{-t/\tau_{delayed}}) \tag{1.2}$$

Any energy remaining in a vibrational state is not in equilibrium with the rest of the lattice and quickly decays down to the lowest vibrational state at room temperature, which is roughly 0.025 eV [20]. An important consequence of this energy level scheme is that once light is emitted, it is difficult to be re-absorbed, due to the presence of vibrational levels. This causes the scintillation material to be mostly transparent to its own light, hence scintillating fibres typically have long attenuation lengths.

Organic scintillators have a defining benzene ring in their molecular structure and can be further subdivided into three groups: organic crystals, liquid scintillators and plastic scintillators [22]. Plastic scintillators are typically moulded into a block, a sheet or a fibre optic cable to be used for various purposes. Additionally, plastic scintillators are safe to handle as their core is made from polystyrene (PS), and their cladding (if present) is made from Poly(methyl methacrylate) (PMMA - also known as acrylic), and which are simple plastics.

Scintillating fibre optics in particular can be used for particle tracking. In this case, a particle hits a specific fibre and activates it, releasing photons which travel down the scintillating fibre and into a light guide. This light must be converted into a usable form, which is accomplished by a light collection device.

Being able to mould scintillating materials into scintillating fibres which have an extremely fast response time (and therefore, an associated low "dead time") makes scintillating fibres a very good choice for building a particle tracker or coordinate detector.

1.4 Light Collection Devices

A pulse of light released in a plastic scintillating fibre after excitation typically lasts for 1-10 nanoseconds. A pulse of such short duration is impossible for a human eye to register, thus, a light collection device is required. These devices collect information about the light pulse and indicate that a particle has passed through a scintillating fibre. There are a few different types of these devices: Avalanche Photodiodes (APD), or a variant of an APD - a Silicon Photomultiplier (SiPM), Visible Light Photon Counters (VLPC) and the most common, Photomultiplier Tubes (PMT).

Each type of light collection device has its own advantages and disadvantages. Some of these important characteristics are:

1. Gain - Defined as the increase in amplitude of an output signal compared to its input signal. In every circumstance a higher gain is preferred, although that may come at a cost.

2. Operating temperature - The temperature required for optimal, or correct, performance of a device. Typically room temperature is desired, however, some devices require a cryogenic cooling system that introduces a large overhead cost.

3. Gain Uniformity - A measure of the gain of different channels within one device relative to the same input signal. A gain uniformity of 1:1 between channels is ideal, however, variations can be accounted for with proper calibration.

4. Operating Voltage - The input voltage required for optimal, or correct, performance. Most devices have a range of voltages in which they function, and in most cases there is an optimal voltage.

5. Dark Current - A measure of signal output, even without a signal input. Dark current can usually be accounted for by increasing trigger levels when using the device, to avoid use of "no input" signals. In general, a smaller dark current is preferred.

6. Photon detection efficiency/Quantum Efficiency - This is an important property that is defined by the probability that one photon will release one photoelectron. A higher detection efficiency is always preferred.

7. Cross-talk - This represents the "leakage" of a signal into an adjacent channel within one device. Ideally the cross-talk would be zero.

Other characteristics exist, but the seven mentioned are the most important in choosing a light collection device. Different devices, with their advantages and disadvantages, will now be discussed.

1.4.1 Avalanche Photodiodes and Silicon Photomultipliers

APD's have high quantum efficiency, low packaging costs, ruggedness, adequate insensitivity to neutron damage, and can operate at or near room temperatures [23].

APD's are sometimes cooled to subzero temperatures, as low as -35°C, in order to increase detection efficiency, reduce noise and decrease photon detection threshold [24]. Low noise and low photon detection threshold at low temperatures make APD's suitable for space born experiments. A pitfall is their low gain; APD's used in the Solar Neutron Tracking (SONTRAC) Experiment, while being cooled to -32°C, had a gain of only 1300 [25]. APD's also have a dark current equalling about 20 triggers per second [25]. When operated at room temperature APD's can only have a gain of $\sim$ 450 in order to compensate for the dark current. It has been shown the gain uniformity can be as large as 1:1.25 under imperfect conditions [25].

A derivative of the APD, an SiPM, is a semiconductor device which, when operated above its breakdown voltage, can achieve high gains of $10^5 - 10^6$ [26]. SiPMs have a compact design with many input pixels (32 or 64) allowing them to be packed densely into a small area. The SiPM quantum efficiency ranges from 12% to 20% [26].

1.4.2 Visible Light Photon Counters

VLPC's have an extremely high quantum efficiency, commonly greater than 60% [27]. They can have high gains of 1.5×10^4 [27], a time resolution of less than 100 ps, and low noise . A failing associated with VLPC's is that, in order to function well, they require a cryogenic chamber (called a cassette) that is maintained at temperatures near 6.5 K [27], which can be very costly and difficult to maintain.

1.4.3 Photomultiplier Tubes (PMTs)

PMTs are the most common type of light collection device associated with scintillators, due to their suitability for high beam fluxes. PMTs have a very fast response time of roughly 1 ns [28] and also have a low cross-talk between channels, with a maximum of 4.9%[1] [29]. The latest development in photomultiplier tubes makes use of weak electrostatic focusing and bi-alkali photocathodes, increasing their quantum efficiency [30]. PMTs have a massive gain of up to 4.4×10^6 and have a gain uniformity of 1:1.1 to 1:1.25 [31], meaning channels will differ by no more than 25%. PMTs also have a quantum efficiency up to 25% [26, 32]. Single channel PMTs are typically operated at a high voltage near -1700 V [33], while multichannel PMTs are operated at a lower voltage typically near -1000 V [32]. A diagram for a simple single channel PMT is shown in Figure 1.2.

A PMT functions by absorbing a photon at its photocathode. Through the photoelectric effect, a photoelectron is released if the photon has energy above the photocathode's work function. For PMTs, the work function is less than the energy of an incoming visible photon. The photoelectron is then accelerated towards the first dynode. This is a metal plate held at a positive voltage compared to the photocathode. Typically the first dynode is held near 100 V potential difference with respect to the photocathode, and each subsequent dynode is held at a larger voltage. Once the photoelectron strikes this first dynode, 3-4 electrons are knocked off, and those 3-4 electrons will then each knock 3-4 electrons off the next dynode. This continues until all 12 dynodes (in the case of the H7546B [32]) have been struck.

[1]Maximum channel cross-talk of 4.9% for Hamamatsu H7546B PMTs.

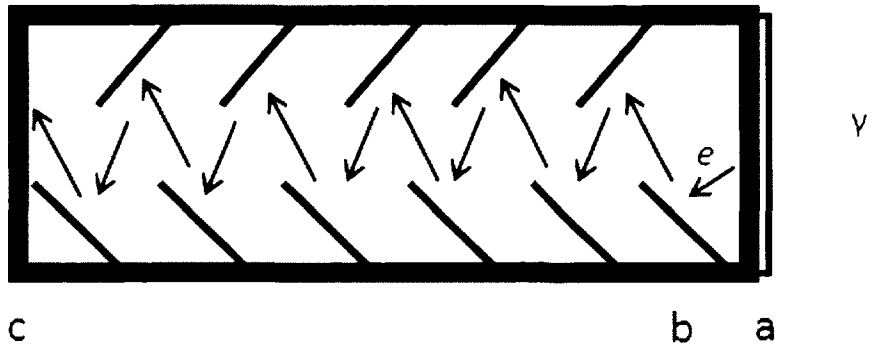

Figure 1.2: The basic operation of a PMT (Photomultiplier tube). (1) An incoming photon strikes the photocathode at (a), where a photoelectron is released. The photoelectron is accelerated toward the first dynode (b) (a metal plate) which has a positive voltage relative to the photocathode. When the photoelectron strikes the first dynode, many electons are released and accelerated towards the next dynode which is held at a larger relative voltage. This multiplication process continues until the electrons are accumulated at the the anode (c) where an electrical signal is produced. This signal can then be processed by high-speed electronics.

The electrons are finally collected on the anode, which is held at the largest voltage relative to the photocathode. This charge collection on the anode results in a signal pulse, typically lasting 10-20 ns, that will be processed by the high-speed electronic equipment.

PMTs can operate perfectly fine at room temperature, while VLPCs [27] cannot, thus giving PMTs this advantage. PMTs having gains of 4.4×10^6 [31] at room temperature also give them an advantage over VLPCs with a gain of 1.5×10^4 [27] (when cooled) and APDs which have gains of 450 [25] at room temperature. To be able to increase APD gain, they must be cooled to decrease noise. PMTs also have a

small channel cross-talk with a maximum 4.9% max [29]. Compared to SiPMs which have a quantum efficiency of 12% to 20% [26]. PMTs have a higher quantum efficiency of up to 25%-30% [14,26,32] allowing them to detect photons with a higher efficiency. In conlusion, PMTs are well suited light collection devices for the majority of nuclear and particle physics experiments, since they have several advantages over all other light collection devices.

1.5 Basic Scintillating Fibre Tracker Design

The basic design of an SFT is quite simple. Typically a number of scintillating fibres are placed in a grid, with fibre planes oriented orthogonally (e.g. x and y directions). A passing charged particle causes a scintillating fibre in each plane to activate. This allows a precise determination of the position of a passing particle. Each fibre needs to be read out by a light collection device in order to cover the entire grid. Additionally, since small fibers are only semi-rigid, a frame or support is required to hold them in place. These requirements can change from use to use, but they are more or less present in every SFT. Some other common elements are described below.

1.5.1 Fibre Bundling

Fibre bundling is sometimes incorporated to increase detection efficiency, however, this can affect spatial resolution and introduce higher fibre costs. Multiple fibres, anywhere from two [27] to twenty-four [11], are placed perpendicular to a particle

beam, in such a way that the incoming beam "sees" only one fibre. Analogously, the first fibre casts a shadow over the others in the bundle. When a particle passes through the first fibre, perhaps undetected, it will then pass in succession through the remaining fibres in the bundle, thus increasing the likelihood of detection.

A common way to describe bundle placement is fibre pitch. This is simply the distance from center to center of two fibres in different bundles (usually columns) as seen along the beam direction. This is shown in Figure 1.3. The column pitch (p) and overlap (o) are determined by [31],

$$p = \phi \cos\theta \qquad o = \phi(1 - \cos\theta) \tag{1.3}$$

where ϕ is the fibre diameter and θ is the column angle. An example of some fibre pitches is shown in Figure 1.3. Typically, columns are defined along the particle beam direction. The theoretical spatial resolution (σ) is given by [31]:

$$\sigma = (\phi - 2o)/\sqrt{12} \tag{1.4}$$

where ϕ is the fibre diameter and o is the fibre overlap defined by Equation 1.3.

Different configurations of layers and overlap can be used to increase particle detection efficiency and increase resolution. However, using extra layers of fibres puts more material in front of the beam, causing more energy loss and trajectory deflection. Having more fibres in a bundle increases the distance between consecutive axis planes, which can decrease spatial resolution as well.

One SFT was constructed using ribbons of scintillating fibres, each con-

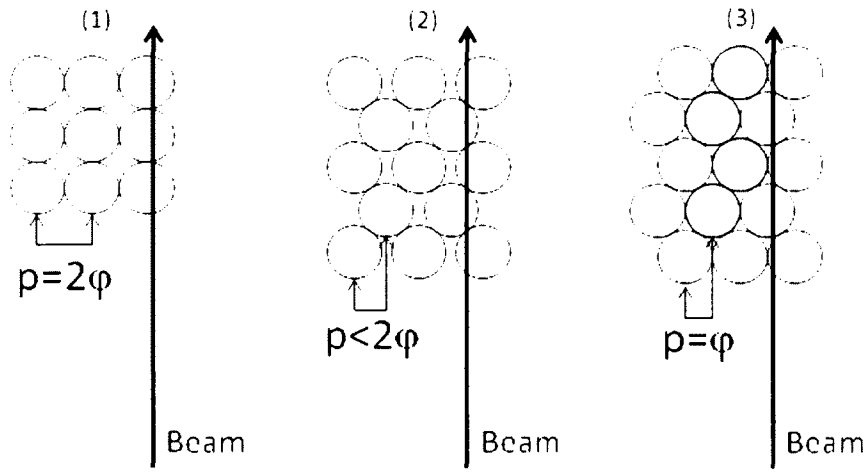

Figure 1.3: Figure pitch from the particle beam's perspective. (1) Fibre centres are separated by 2ϕ, where ϕ is the fibre radius and p is the fibre pitch. (2) $p < 2\phi$. (3) From the beam's perspective, the fibre centres in adjacent columns are separated by only one fibre radius, $\therefore p = \phi$. Columns are defined along the beam direction. This Figure was constructed using definitions defined in [31].

taining five layers of fibres. The detector had a pitch of 275 μm and layers were staggered by half the fibre pitch [34]. Another SFT instead used 24 bundles, each having 24 scintillating fibres, for a total of 576 fibres. The same was done in the perpendicular direction. The fibre read out method was very unique, having one fibre connected to two different PMTs, allowing 576 fibres to be analysed with only 48 PMT channels [11].

The Dimeson Relativistic Atom Complex (DIRAC) detector used 240 read-out channels, each having 5 fibre columns. Each fibre column had a column pitch of 0.43 mm [35]. A similar tracker, The Common Muon Proton Apparatus for Structure and Spectroscopy (COMPASS) detector had two precisely overlapped ribbons of 16

columns each with 7 fibres per column aligned along the incident particle direction [18]. Similarly, another SFT had arranged fibres into two ribbons of ten columns with three fibres each. The columns of three fibres were then hooked to an SiPM [14]. Rather, another SFT had four fibres in a row aligned along the beam direction, which defined the bundle, with a fibre pitch of 0.59 mm [36].

This information shows that most groups aligned fibres perpendicular to the incoming particle beam direction, while it is also possible to align them along the beam. It has also been demonstrated that a number of configurations are available, and should be matched with the specific task an SFT is required to perform.

There are two main types of SFT frame layouts: cylindrical and rectangular. For detectors requiring a beam or interaction site to be enclosed with an SFT, a cylindrical detector can be used. In another case, a specific scattering angle may want to be investigated. A rectangular frame would benefit this need, eliminating the cost of fully enclosing the interaction region.

Cylindrical Design For experiments requiring a barrel of scintillating fibres to enclose a beam, or target, a cylindrical design can be used. An SFT was designed for vertex detection where a cylindrical shell of scintillating fibres was built to surround a particle beam line. Three layers were used, one parallel to the beam line, and two others at $\pm 45^{\circ}$ to the beam line. This provided nearly a 4π view of the beam line and collision. Experimenters were then able to trace back the trajectories of the detected particles to find the interaction vertices [37]. In another experiment, for the DØ detector at Fermilab, a cylindrical like approach was used. 3072 scintillating fibres were arranged into 24 singlet layers, 128 fibres wide. Three different orientations

were used, x, u and v. The u and v planes were oriented at an angle of $\pm 2^{\circ}$ to the x plane. Each plane was in a doublet configuration, meaning that two layers had the same orientation, just offset by half the fibre diameter, which was $\phi = 0.835$ mm [27]. Similarly, an SFT was designed for the Hadron-Electron Ring Accelerator Measurement of Spin (HERMES) recoil detector which consisted of two concentric cylinders of scintillating fibres around a beam line with 4992 read-out channels between the two cylinders. Each cylinder had four fibre layers, two parallel to the beam direction and two at an angle of 10° [38].

Rectangular Design In many experiments a beam will pass through a coordinate detector positioned some distance from the interaction location. In this case, it is more cost effective for an SFT to be of rectangular design. An example of such a design is provided in [28] from Jefferson Lab's Hall B. This SFT was constructed with an aluminium rectangular frame with dimensions 44.45 cm x 21.59 cm x 3.81 cm. The active area, where the scintillating fibres interact with the particle beam line, had dimensions 13.97 cm x 13.335 cm and was covered with a single sheet of matte black Tedlar. The purpose of the Tedlar sheet was to keep out ambient room light while minimizing the material the particle beam would encounter. The aluminium frame was also covered with a matte black paint to reduce reflections. Rubber O-rings were placed between the SFT and the holding frame to ensure optical isolation. An electronics housing frame was also designed and built to be easily accessible so the read-out electronics could be removed for repair without disturbing the scintillating fibre array. The fibres were then held in place with three plastic Delrin jigs [28].

It has been demonstrated above that many examples exist of different

types of fibre frames shapes. with different pitches and overlaps. Experimenters and designers must optimize the different SFT parameters available to them.

1.5.2 Scintillating Fibre to Light-guide Connector Modules

When dealing with large numbers of scintillating fibres, being able to efficiently connect them to the light guides is crucial. The amount of time put into detector construction can be drastically reduced if an efficient coupling method is found. Some of these methods are detailed below. It should be noted that nearly all light collection devices use the same fibre to photocathode method, that being a plastic "cookie" which has one hole for each pixel [14–16, 18, 25, 29, 30, 35, 39–42]. When fibres are inserted to their respective holes, they are typically secured by glue, then the cookie is attached to the front plate of the light collection device.

One group [43] used a Delrin plastic v-groove connector to reduce machining and to eliminate the need to thread individual fibres into holes. The connector attaches two layers of 64 scintillating fibres to two layers of light guides. The chassis had two mating sets with three pieces in each set, a center piece with 64 v-grooves on the top and bottom of it, and two top and bottom bars having flat surfaces. The fibres were laid into the grooves and clamped in. There is also a glue pocket to insert glue. Once the fibres are laid and glued, two screws clamped the scintillating fibres and light guides together. A 97 - 99% light transmission was achieved for all fibres [43]. This design is a simple and efficient way to couple scintillating fibres to light guides resulting in a very high light transmission efficiency.

1.6 Common SFT Design Elements

When constructing an SFT, a number of choices must be made in order to optimize the detector for its particular use. However, certain aspects of the design are consistent across different uses. These commonalities include: (1) Scintillating fibre coating, (2) optical coupling, (3) fibre-end finish and (4) reflective ends.

1.6.1 Scintillating Fibre Coating

The scintillating fibre component of the detector needs to be in a light-tight enclosure, otherwise photons will continually activate the scintillating fibres which will in turn activate the light collection device and appear as real events. Another possible source of false events is from photons "leaking" from fibres. As ionizing particles pass through the scintillating fibres, scintillation light is released isotropically. Some of the produced photons will escape the fibre and possibly enter into an adjacent fibre. If an adjacent fibre is activated by such "leaked" scintillation photons, the position resolution is decreased and/or interpretation of the event is compromised, since now two fibres are activated (which is an unwanted effect[2]).

One study has investigated the cross-talk effects of leaking photons in single and double cladding scintillating fibres [35]. It was demonstrated that single cladding scintillating fibres required additional light coating, while double cladding fibres did not. It was also found that the cross-talk between double cladding fibres was $\sim 5\%$. However, no experiment was done to compare the cross-talk of coated fibres versus

[2]This unwanted cross-talk effect is not to be confused with the idea of fibre bundling. In the fibre bundling case, it is desired to increase detection efficiency by purposely allowing a passing ionizing particle to hit multiple fibres.

uncoated fibres. The cross-talk was measured between adjacent fibres that were single cladding in one experiment (designed for the DIRAC detector) and double cladding in another (designed for the COMPASS detector). Unfortunately, the detector set-up was not the same between the two experiments, leading to more experimental parameters that were not necessarily held constant. The single cladding fibres had five fibres in a column, while the double cladding had seven fibres per column. Also, the single cladding fibres were attached to clear light guides before being read out by a PMT, while the double cladding fibres were not. This is a significant difference between the two experiments because there may have been other cross-talk effects occurring at the scintillating fibre to light guide interface. The conclusion of this study indicates that one way of reducing cross-talk between fibres is to use double cladding scintillating fibres instead of single cladding scintillating fibres.

Another study completed comprehensive research into the effects of coating fibres [39]. Multi-cladding 2 mm x 2 mm square scintillating fibres[3] were used, and it was shown that white extra-mural absorber (EMA) coating on scintillating fibres reduced the number of photoelectrons released from a photomultiplier tube. An explanation for the reduction in the number of photoelectrons was given:

"Cladding light travels about a 1/4 wavelength outside the cladding every time it is reflected through total internal reflection. When EMA is present, and especially when this EMA is black, a large fraction of the cladding light is absorbed in the EMA and the attenuation length for the cladding light is drastically shortened, to the point that even a few cm away from the PMT it does not contribute to the

[3]Model: Bicron BCF-12MC

collected signal in any significant way" [39].

This means the photoelectron count drops off quickly as particles pass through the scintillating fibre at increasing distances from the PMT, and then levels off at further distances, and remains nearly constant. That said, the photoelectron count for EMA coating at any distance (up to 70 cm distances were tested) is smaller than the photoelectron count without coating. Unfortunately, no cross-talk effects were investigated. This group decided to use coated fibres, presumably because reducing cross-talk was more important than increasing the detection efficiency. This group demonstrated that coating fibres does reduce the signal arriving at the light collection device. This effect may be an important consequence to some experiments where the maximum collection of light is more important than reducing cross-talk. This is operating under the assumption that cross-talk is reduced with fibre coating, which wasn't explicitly measured in this study.

In support of the immediately aforementioned experiment [39], another group reported that painted scintillating fibres have a lower detection efficiency and higher resolution than unpainted ones [17]. Test fibres with a 0.5 mm radius that were painted and unpainted had 2 mm and 2.6 mm resolution (at full-with-half-maximum) respectively. The corresponding particle detection efficiencies were 1.3% and 1.9%, respectively. This result should apply to most SFT projects, however, it was done in 1992, and the experimental process was not very detailed in the publication. Many aspects of fibres and light collection devices have changed since then. The SFT was also extremely tightly packed, even between different axes, which is not always common in SFT.

When coating scintillating fibres, the ultimate goal is to reduce cross-talk in the system. Other alternatives to coating exist which could possibly accomplish the same result of reducing cross-talk. One group [44] studied the collection of scintillation light using a photomultiplier tube; instead of coating, a 0.01 mm thick Mylar film[4] was wrapped in an accordion fashion between fibres to reduce cross-talk effects. Another example is a group [45] that coated fibres with black paint, a few micrometers thick and covered the detector array with a Mylar sheath, to prevent possible reflections from the aluminium structure. One SFT was constructed and its scintillating fibres were coated with a standard white diffusing coating[5]. Another example was from a group that used Stycast epoxy loaded with 20%-33% TiO_2 to prevent cross-talk between fibres [34]. Other groups also used EMA coating to attempt to reduce scintillating fibre cross-talk [46].

While these were indeed novel approaches, no tests were completed (at least, no such tests were reported) to support the papers' use of different cross-talk reduction techniques. More investigation must be done to determine the effectiveness of these different coating and light blocking techniques on scintillating fibre-to-fibre cross-talk. Experiments using black paint have been carried out for this thesis. The experiment, results, analysis and conclusion are presented in Chapter 2: Effects of Fibre Coating on Adjacent Scintillating-to-scintillating Fibre Cross-talk.

[4]A reflective plastic film made from polyethylene terephthalate.
[5]BC-620 from Bicron Corporation.

1.6.2 Optical Coupling

Scintillating fibres typically need to be coupled to light guides, then the light guides need to be coupled to a light collection device. This can be done in a number of ways, including optical epoxy, optical grease, silicon plugs, an air gap or UV cured glue. Depending on the specific needs of a certain fibre tracker, different coupling methods may perform better under those constraints. For example, a detector may already have a rigid frame where fibres are inserted and held in place; in this case, a non-rigid coupling, such as air or grease, may be acceptable. In contrast, if a detector did not have a specific holding block to connect light guides to scintillating fibres, then a rigid coupling, such as optical epoxy, may be needed.

This section is broken into two categories: (1) coupling scintillating fibres to light guides, and (2) coupling light guides to light collection devices.

Coupling of Scintillating Fibres to Light Guides When coupling a scintillating fibre to a light guide, essentially any optically transparent couplant can be used, depending on the type of detector being built. A number of different different groups have reported light guide to scintillating fibre interfaces being optically connected using optical epoxy [18, 27, 35, 39].

One group [27] reported inserting 128 fibres into a large plastic connector. Each fibre had its individual hole, then optical epoxy was applied and light guides were inserted into the opposite side of the plastic connector. The light transmission through the plastic optical connector, using optical epoxy as the couplant, was measured to be 95% [27]. Also, slightly larger diameter light guides than scintillating fibres were used

in order to capture as much light as possible exiting the scintillating fibres [27]. No investigations were done to determine the benefits of using larger diameter light guides in that experiment. However, another group has investigated the light yield between a light guide and scintillating fibre connection by adjusting axial misalignment, gap-width and axis angle between connecting fibres; they found that increasing any of these parameters causes drastic light yield drops [47].

In contrast, another group reported using optical grease at the scintillator/light guide joint [43]. The different coupling method is most likely due to rigidity not being required in the latter since a solid Delrin plastic frame was used to secure fibres. Ultraviolet curing glue[6] has also previously been used to secure scintillating fibres to light guides [28].

One group did research on optical couplants and collected data in 1996 [43]. This data may potentially be outdated, due to developments in the field; however, some noteworthy conclusions and observations were made. It was noted that optical grease works well in temperature-controlled environments, and is preferred over mineral oil due to its viscosity. For long term coupling, a solid couplant is preferred to reduce the effects of the couplant flowing away. A 98% average light transmission efficiency was found for optical grease [43].

Experiments using different optical couplants has been completed for this thesis. The experiment, results, analysis and conclusion are presented in Chapter 3.

Coupling of Light Guide to Light Collection Device All light collection devices have a photocathode at the fibre input end. Due to the high cost of individual

[6]Model 3094 adhesive and a PC-3 UV lamp from Dymax corporation

light collection devices, some experimenters may not want to damage the photocathode by gluing fibres to it. To get around this, a holding block (or "cookie") is used to hold fibres in place, and the photocathode end of the fibre is coated with an optical couplant. Since optical grease, mineral oil or air, does not damage the photocathode there may be a bias in this section favouring those types of couplants.

Some groups have connected test fibres to light collection devices using optical grease [23, 45]. Others did not use any optical interface to connect fibres to the PMT [18, 31]. Interestingly, it has been shown that optical epoxy had a 15% higher light yield than optical grease when attaching light guides to the photocathode of a PMT [35].

Although one would assume there is no difference when connecting fibres to a PMT, APD, SiPM or VLPC, it is possible different photocathode materials bind differently to various optical couplants. These examples show more investigation may be required into which optical couplant is optimal, and which pairs best with different light collection devices.

1.6.3 Fibre Finish

When preparing a scintillating fibre to be secured to a light collection device or a light guide, the fibre's finish must be considered. More specifically, does it need a rough finish, which could be accomplished by course sand paper, a smooth finish, a polished finish or just be cut by scissors. Arguments can be made in favour of each type of finish (e.g. a rough finish allows opportunity for optical epoxy or grease to "fill in" the roughness to provide good light transmission; or, a scissor cut is

the least expensive method). While investigating the literature, only one reference described their fibre finish in detail, while a few others highlighted that they did indeed polish their fibres. However, no comparison of the different finishes was found. This construction element is important because it directly affects light transmission. If light is lost at the scintillating fibre/light guide boundary, that information cannot be recovered. This may also provide a cross-talk mechanism, since light that leaks could enter an adjacent scintillating-to-light guide interface; however, this cross-talk effect has not been investigated. Further, there are differing levels of effort and expense related to the different finishes, and choosing the least expensive (or easiest) method that provides adequate light transmission is preferable.

Extensive effort has been put into polishing scintillating fibres by one group [28]. In order to achieve the necessary level of smoothness on fibre ends, finer and finer grit sand paper was used (30, 9, <1 μm granules). After sanding was completed, a final high gloss polish was applied using a 0.05 μm aluminium oxide water-based slurry. While fibres were being polished, a 400 grit wetted sandpaper was used to remove excess material. During the process, fibres were held in place after being inserted into a hole drilled through the central axis of a Teflon rod (1.905 cm x 5.08 cm). Other collaborations have also polished fibres [31, 34, 45], yet still no experimental evidence was given to show this is necessary.

This thesis addresses this knowledge gap in the literature. The experiment, results, analysis and conclusion is shown in Chapter 3.

1.6.4 Reflective Ends

Another technique to increase photon yield at the end of a scintillating fibre is available. This technique involves coating the non-read out end of the scintillating fibre with a reflective material. The theory to why this technique works is as follows. when a particle hits a scintillating fibre, photons are emitted isotropically, a small percentage of the photons will travel down the fibre in both directions. This small percentage is called the trapping efficiency and is defined as the percentage of a full 4π sphere of light that is trapped inside a fibre. The trapping efficiency for single and double cladding fibres is typically $\sim$3% and $\sim$5% respectively [31]. The same amount of light travels down the fibre in opposing directions. The light travelling toward the non-read-out end will encounter a reflective barrier and switch directions back towards the light collection device, increasing the photon yield. In order to accommodate this change, either the high speed electronics reading out the light collection device needs to be set up to allow the collection of two bursts of photons, or the fibres need to be short to minimize the time between photon bursts to allow data collection during a single timing/trigger gate.

One involved study into the effects of coating fibre ends has been carried out [39]. The amount of photons arriving at the end of fibres was observed for two scenarios: (1) terminating the open end of scintillating fibres with vacuum deposited aluminium, and (2) applying a Mylar film to the end of fibres. Results indicated that using Mylar increased the photoelectron count by 5-10% over aluminium. It was also shown that fibres terminated with a mirror have a 20-40% higher photoelectron yield than a non-mirrored counter part. In agreement with the fact that reflectors

increase photoelectron yield. it was seperatly concluded that aluminized Mylar reflectors increased light collection devices signals by 60% [25]. however, different types of reflectors were not compared.

A few different approaches to the same technique include:

1. Applying Aluminium to the free end of scintillating fibres [31]. A vaporization chamber was used that had an electric oven inside to heat a pellet of aluminium. The aluminium would evaporate and adhere to the free end of the scintillating fibre. An increase in light yield of roughly 50% was found after applying aluminium to the free fibre end.

2. Applying an aluminized Mylar mirror to the the non-read-out scintillating fibre ends [27]. This allowed the passage of Light Emitting Diode (LED) light for testing, but reflected the majority of scintillating light. In a similar way to applying aluminium, the open end of scintillating fibres used were tightly pressed to an aluminium mirror, which was vacuum evaporated onto a PMMA plate [35]. Likewise, a sheet of aluminized Mylar has been glued to the open ends of fibres [18].

3. Covering non-read-out fibre ends with a reflective foil [14].

4. Placing a mirror over free scintillating fibre ends [34].

This portion of the literature seems complete. There are some minor differences between whether a Mylar film, an aluminium film or a aluminized Mylar film should be used, but the results are available, and they are up to date. Three conflicting reports suggested that aluminium [31], Mylar film [39], and aluminized Mylar

film [25] applied to fibre ends are all the best reflectors. Although these experiments did not directly test all three popular fibre-end reflectors, an experiment comparing these choices would contribute to the literature. Consequently, it has been adequately shown that fibres with a reflective fibre-end have a significantly higher light output than those not using a reflective end.

1.7 Types of Scintillating Fibre

A multitude of different scintillating fibre types are available on the market today, in a number of sizes. There are two main shapes, circular and square, where the former is much more common (although square fibres are not rare). There are two main producers of scintillating fibres, Kuraray [48] and Saint Gobain Crystals [49] (formerly known as Bicron [50]). Fibres are available in a variety of attenuation lengths, depending on their dopants and cladding. Attenuation length is defined as the distance light must travel in a fibre to fall to $1/e$ (36.7%) of its original intensity. For the most common scintillating fibres, this is in excess of 3.5 m. Another important aspect of scintillating fibres is the numerical aperture (N.A.) which is equal to [51]:

$$\text{N.A.} = \sqrt{n_{core} - n_{cladding}} = \sin(\alpha/2) \tag{1.5}$$

where n_{core} and $n_{cladding}$ are the indices of refraction of the core and cladding, and light leaving the fibre spreads out into a cone of angle α. This is important when trying to match a fibre to a light collection device, or a light guide. Some conclusions have been made and are discussed in this section, such as: circular versus square fibres,

the effects of radiation on fibres, and matching fibres to light collection devices.

When choosing a scintillating fibre, one must consider matching it to the light collection device. Within a scintillating fibre, light is released with a range of wavelengths and there is a peak emission wavelength where the majority of light is emitted. Light collection devices have a similar feature called peak sensitivity wavelength, which is the wavelength of light that produces the biggest signal in the light collection device. Typically, the peak emission wavelength and peak sensitivity wavelength is in the blue or green region. The signal amplitude produced by the light collection device is maximized when the fibre's peak emission wavelength is matched with a light collection device's peak sensitivity wavelength.

Various scintillating fibres have been tested [42] by looking at the multi-channel spectra of fibres when a ^{90}Sr β-source was placed 50 cm from the PMT. It was found that 2 mm diameter fibres had five to eight times more event counts than 1 mm diameter fibres [42]. A single photoelectron signal was found in all trials. These spectra can be observed when data is collected using an Amplitude-To-Digital Converter (ADC) from many events, a type of graph called an ADC spectrum. It is useful to view the ADC spectrum to better understand how the SFT functions.

Another property of scintillating fibres is radiation hardness. Although this property has no numerical value, looking at different properties such as the attenuation length after exposure to radiation gives an idea of the fibre's radiation hardness. The effects of radiation on attenuation length have been investigated by irradiating various Bicron scintillating fibres [52]. It was found that soon after receiving an 80 krad dose, the attenuation length of fibres decreased by about 10%. Also, fibres doped

with p-terphenyl-3-hydroxyflavone (pT-3HF) recovered to their original attenuation length after one day of air exposure. Similar results were also found over a two year study for the Superconducting Super Collider (SSC) [53].

During the construction of the SONTRAC SFT, a new prototype SFT, it was noted that square fibres were difficult to use when compared to circular fibres [54]. A number of square fibres became twisted and did not end up in the proper position, where circular fibres would have. This twisting caused irregularities in the spacing between fibres and may have been detrimental to the tracking capabilities of the detector.

In conclusion to these reports: circular fibres are easier to use than square fibres; large amounts of radiation have only small effects on the attenuation length of fibres; and, fibres should have wavelengths matched to light collection devices. These conclusions were used when selecting scintillating fibres for the experiments presented in Chapters 2 and 3 of this thesis.

1.8 Experimental Designs

In order to perform the experiments that are described in Chapters 2 and 3, it was necessary to investigate different methods that have been used to perform similar experiments. The two experiments that have been performed for this thesis are: (1) The effects of fibre coating on adjacent scintillating fibre cross-talk, and (2) the combination of different fibre-end finishes with different fibre couplants and their effects on light transmission. The former requires fibres to be activated by a radioactive source in order to determine how much cross talk exsists. The latter is

simply measuring the light transmission between scintillating fibres and light guides for different fibre-end finishes and optical couplant combinations. Key features of the two experiments described below have been used as a base to perform the experiments for this thesis.

An experiment was performed to determine the attenuation length of 4 m long, 0.875 mm diameter Bicron G2 scintillating fibres [23]. An APD read-out and a ^{106}Ru β-source was used to activate the fibre. The β particles travelled down a collimator, of 0.4 mm diameter, where the scintillating fibres were placed, perpendicular to the β path. The first and last fibre traversed by the β particles were the triggers, and the test fibre was between them. Thus, if all three fibres have a signal present, the test scintillating fibre was read out by an APD, and the signal was collected by the electronics. The test fibre was able to move in and out of the collimator in order to change the distance from the interaction region to the APD. The attenuation length of the fibres was found to be 482 cm.

Another experiment tested the output of a prototype SFT for the Jefferson Lab tagged photon beam line [28]. An SFT was tested using two scintillating paddles as triggers and a 5 μCi ^{106}Ru β-source to produce minimally ionizing particles (MIP). A MIP is a particle that when passing through matter will lose energy at a rate of (or close to) $\partial E/\partial x \sim 2$ MeV/g cm^2, which is the smallest possible rate for all particles [22]. Each fibre was read out using an R2249 Hamamatsu PMT, where a typical output between 18-20 photoelectons was found for each MIP with no more than a 15% variance between fibres.

The important features to take from the aforementioned experiments are:

1. Having a top and bottom trigger eliminates the need to read out the electronics every time a test fibre is activated. It also assures the experimenter that the interaction region is between the two triggers. The top and bottom trigger technique has been used for the experiments in this thesis. The technique proved very useful in data reduction and ensured that particles passing through test fibres in a region of non-interest were ignored.

2. If a large interaction region is required, scintillating paddles (also called plates) can be used as triggers.

1.9 Refined Goal of Thesis

The refined goal of this thesis is to: (1) Investigate the effect on adjacent scintillating-to-scintillating fibre cross-talk by coating scintillating fibres with a light tight coating: and, (2) Investigate the effect on light transmission from the combination of different fibre-end finishes and clear-to-scintillating fibre optical couplants.

Chapter 2

Effects of Fibre Coating on Adjacent Scintillating-to-scintillating Fibre Cross-talk

In an SFT, adjacent scintillating fibres are so close to each other that light may leak from one fibre to the next. These "leaking photons" can be a source of cross-talk due to the fact that scintillation within a scintillating fibre will release photons isotropically, possibly leaking into an adjacent fibre and activating it. Since a typical single cladding scintillating fibre has a trapping efficiency of only $\sim$ 3% [31], the majority of light is not trapped in the fibre and is leaked. Even though scintillating fibres are mostly transparent to their own radiation, a small number of matching energy levels are still present and may be excited.

It was hypothesised that coating scintillating fibres with a light tight coating will decrease the amount of scintillating-to-scintillating fibre cross-talk.

An experiment has been performed to compare the cross-talk between eight painted fibres, and under identical test conditions, eight unpainted fibres. The eight fibres in both tests were positioned adjacent to each other in a plane, and were directly routed to a PMT. A number of radioactive sources were used to activate the fibres.

2.1 Experimental Setup: Cross-talk

The experimental setup was designed in order to maximize the collection of data to test the hypothesis while minimizing noise and extraneous variables.

The basic setup is as follows: Ionizing particles passed through a top scintillating plate (S1), then through a scintillating fibre (SF) inside a light tight enclosure, then exited through a bottom scintillating plate (S2). Once all three of these scintillators, S1, SF and S2 were activated, the electronics were triggered for data collection. A schematic of the experiment is shown in Figure 2.1. In order to ensure that one passing particle did not activate two scintillating fibres (SF), the scintillating plates (S1,S2) needed to be positioned in a certain way. They were positioned so that the shallowest angle that a particle could pass between the plates and fibres did not pass through two fibres. The mathematical derivation and figures are shown in Appendix B.

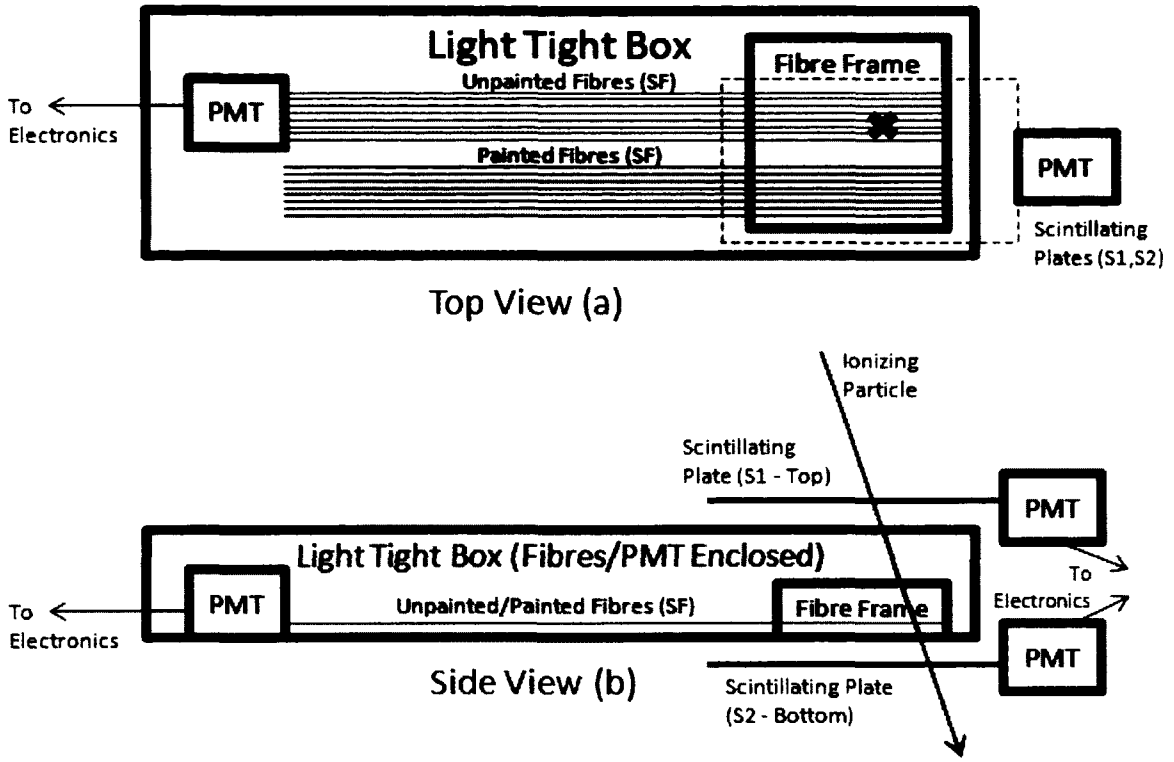

Figure 2.1: (a) The top view of the cross-talk experiment setup. Ionizing particles pass through a scintillating plate (S1) from above, triggering the electronics. The particles then pass through scintillating fibres (SF) then exit through a bottom scintillating plate (S2). The same can be seen in (b) from the side view. With this setup, it is very unlikely that two fibres are hit simultaneously by a passing particle. For a derivation of minimum plate separation, see Appendix B.

2.1.1 Fibres and PMT: Cross-talk

1 mm diameter, 0.5 m long, BCF-20 scintillating fibres purchased from Saint Gobain Crystals [49] were used in the experiments. The scintillating fibres had emission in the green region with a peak wavelength of 492 nm. The fibres also had a 2.7 ns decay time, an attenuation length of > 3.5 m, and could produce ~ 8000 photons per

MeV of energy deposited by a passing MIP. Fibres were inserted into a 64 Channel Hamamatsu H7546B PMT that had a spectral response of 300-650 nm and a maximum response wavelength of 420 nm. The PMT had a gain of $\sim 1.5 \times 10^6$, and a typical uniformity of 1:2.5 [32]. The H7546B PMT was powered by a Matsusada JB-1.5N power supply [55] that was assembled inside a Nuclear Instrumentation Module (NIM) for easier mounting and power connection. This power supply provided a low noise of 1 mV peak-to-peak when operated at 1000 V and very high stability of 15 parts per million. For S1 and S2, BC-400 scintillating plates [49] were used that had an emission spectra of 410-430 nm in the blue region. S1 and S2 were optically coupled to Burle 8575 PMTs [56].

After preliminary results were found (discussed later in Section 2.4), it was noted that light leaked to adjacent PMT pixels at the face of the PMT. This resulted in the need to change fibre placement on the PMT. The fibres were initially lined up in rows of eight, but were moved to maximize PMT face separation as shown in Figure 2.2.

After fibre placement was optimized, the amount of light leaking from an activated fibre's pixel at the face of the PMT to another pixel was minimized.

2.1.2 Read-out Electronics

S1 and S2 are identical scintillating plates connected to identical PMT's. The scintillating plates had a peak emission wavelength in the blue light region. The peak wavelength sensitivity of the PMTs matched the peak emission wavelength of the plates in order to maximize signal amplitude output from the PMT. Ten signals

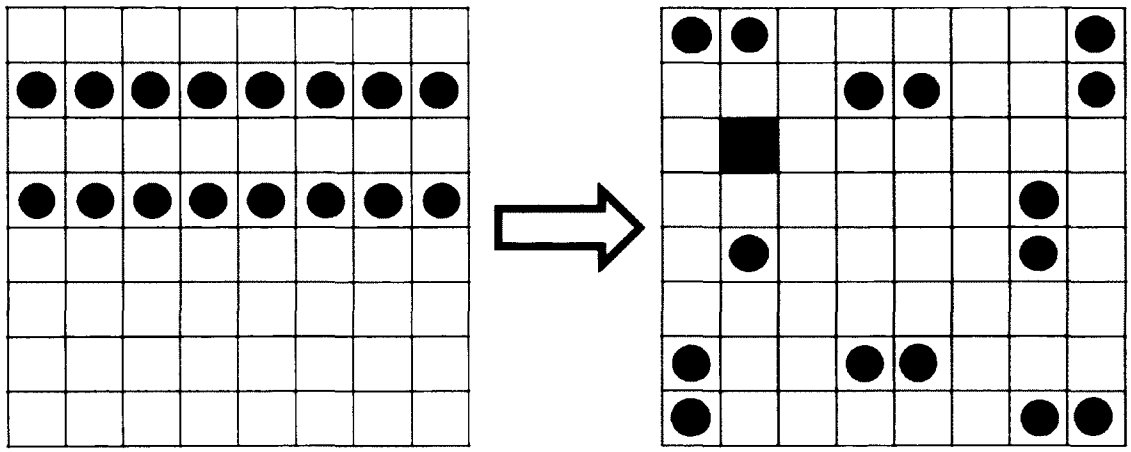

Figure 2.2: Fibre placements on the face of the PMT. Preliminary results shown in Section 2.4 show that the left panel was a poor fibre placement scheme. The right panel shows the corrected and separated fibre placement. Black circles represent locations of painted fibre placement, while open circles represent unpainted fibres. Note the accidentally misplaced fibre that was not noticed until after the experiment was completed.

S1, S2 and eight SFs were fed into a series of electronic modules. The eight SF signals were separate signals that each followed the same electronic path through the modules. The notation SF1, SF2,... SF8 will be used to differentiate between individual scintillating fibres when needed, and SF will refer to all eight scintillating fibres.

Figure 2.3 shows a schematic of the electronics used in this experiment. The signals were fed, using identical length cables, into a Phillips Scientific NIM Fan-out module [57]. The Fan-out (a) was designed to replicate an incoming signal into four identical outgoing signals (including analog signals), in this case four identical

PMT output signals for each of the eight fibre signals. One output of the Fan-out was directed to the input of a Phillips Scientific NIM Octal Discriminator [58]. The Discriminator (b) produced a NIM logic "true" output pulse that persisted a set time after the input signal rose above a set threshold level. The output pulse duration was set to 50.4 ± 4 ns, in order to accommodate the processing time of the the logic units (c,d,e). Table 2.1 shows common standard logic levels used throughout this experiment and the next, described in Chapter 3. The Discriminator voltage threshold ($V_{Thres.}$) for experimental trials was set to -15.0 ± 0.1 mV for SF, and -89.7 ± 0.1 mV and -82.7 ± 0.1 mV for S1 and S2 respectively.

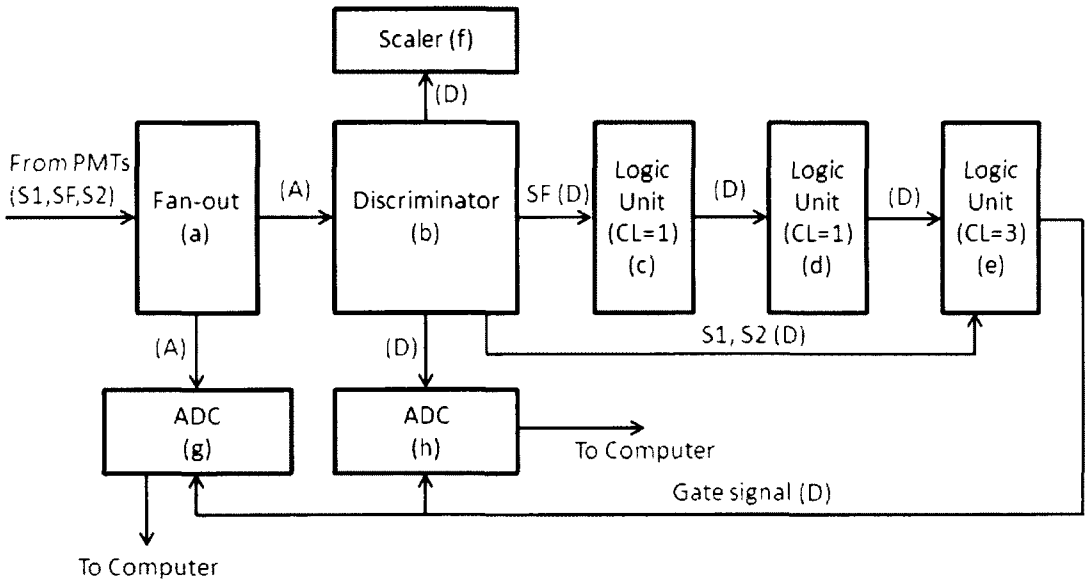

Figure 2.3: This Figure represents the signal flow through the electronics. The letter under the module name is for reference. The letter in brackets next to arrows indicate the type of signal: (A) Analog or (D) Digital. With reference to Figure 2.1, SF corresponds to the eight scintillating fibres, S1 is the top scintillating plate and S2 is the bottom scintillating plate.

Another output of the Fan-out was delayed and fed into a Lecroy ADC (Analog to Digital Converter) [59]. The ADC module integrated the voltage over time of the incoming signal to find the total charge carried by the raw signal[1] pulse then output stored a readable number that is a multiple of 0.25 pC. The total charge was proportional to the energy deposited by a passing particle. A third output from the Fan-out had the option of being viewed by an oscilloscope for debugging purposes.

Type of Logic	Off/False Value (v)	On/True Value (v)
NIM	0.0	-0.8
TTL	0.2	2.5
ECL	-0.8	-1.6

Table 2.1: This table shows voltage levels of the On/True and Off/False states of common logic types used throughout these experiments. NIM - Nuclear Instrument Module, TTL - Transistor-Transistor Logic and ECL - Emitter-Coupled Logic. This information is found in [22].

An output of the Discriminator module was sent into a Phillips Scientific Logic Unit [60] which produced a "true" output pulse if a set number of input signals were "true", and lasted an adjustable duration that was set to 50 ± 4 ns. The logic gates were configured so that if both S1 and S2 were "true", and one or more of the eight SF's were "true", an output pulse was generated; this situation will be considered an "event". An event can be written mathematically, using Boolean algebra, as: S1·S2·(SF1+SF2+...+SF8). This was accomplished using a series of

[1]Raw Signal: A signal that originates from a PMT, due to a photon pulse arriving at the PMT's photocathode. This signal is typically replicated by a Fan-out module and analysed by an ADC.

logic units. Another Discriminator output was sent to a Kinetic System Scaler [61]. The Scaler simply counts the number of "true" values it receives while the experiment is running. One more Discriminator output was delayed by $\sim$ 50 ns and fed into a second ADC. The data collected by the second ADC showed which fibres were activated during an event, since only signals with a voltage larger than $V_{Thres.}$ cause a discriminator output pulse.

Output from the final logic unit was fed into the gate input of the two ADCs. While the gate signal is "true" the ADCs integrated the analog inputs and returned a number which was retrieved by the computer. The reason the ADC analog inputs needed to be delayed was so the logic units had time to determine if an event occurred, taking $\sim$ 50 ns. There were two cascades of logic units that introduced 20 ns of delay, and a total cable delay of $\sim$ 15 ns. The delay caused by light travelling down different path lengths inside a scintillating fibre or plate accounted for 15 ns of delay. The total module, cable and light travel delay could be as large as $\sim$ 50 ns. Hence the reason for $\sim$ 50 ns of delay to the ADC inputs.

The physical setup is very simple and elegant as shown in Figure 2.1, leading to easy diagnostics and troubleshooting. The electronics setup, as shown in Figure 2.3, is more difficult to troubleshoot due to the sheer number of cables, adapters and modules; however, many steps were taken to facilitate necessary diagnostic checks to ensure accurate timing and appropriate signal transfer. Additional technical information about the electronics setup is included in Table A.1 for reference.

2.2 Calibration

This section will present steps taken to calibrate the experimental setup. The smallest real signal (SRS) was determined in order to set $V_{Thres.}$ on Discriminators, and accidental coincidences are investigated mathematically to determine if they would have any role interpreting the results.

2.2.1 Discriminator Threshold $V_{Thres.}$

The Discriminator threshold voltage, $V_{thres.}$, needed to be set properly to ensure that all real signals were received to be analysed and to reject noise. If $V_{thres.}$ was set too high then true signals be missed, and if $V_{thres.}$ was set too low then noise may have incorrectly registered as true events.

In order to set $V_{thres.}$ on the Discriminators, the peak voltage of the SRS needed to be found. The SRS is the smallest electronic signal produced by a MIP passing through a scintillating fibre. By setting $V_{Thres.}$ too far above the SRS, events would be missed. Another reason to find the SRS was to eliminate false signals arising from noise, since the noise level is smaller than the real signals.

In order to determine the SRS, two radioactive sources were placed on top of S1: ^{60}Co (Primary decay mode: $\beta-$ [62]) and ^{22}Na (Primary decay mode: $\beta+$ [62]). This allowed emitted particles to pass through S1, SF then S2 and activate them. Two sources were used simply to increase the rate of MIPs passing through the detectors, since the radioactive sources available were not intense. The scintillating fibre signals were connected to channel A of a BK Precision Model 2540 oscilloscope [63] to determine the SRS. The real signals were observed when the oscilloscope was

triggered by a signal originating from the bottom plate; this bottom plate trigger signal was connected to channel B, and was set to not appear on the oscilloscope display, since it was not needed for observing the SRS.

By using the persist feature on the oscilloscope, the display became populated by large number of signal curves from the SF (channel A). The area under the curve for each of these lines was directly proportional to the charge collected by the ADC. Ideally, there is a distinct gap between the noise level and the SRS. Once the SRS was found for all eight scintillating fibre channels, the Discriminator $V_{thres.}$ was set slightly lower. The SRSs and Discriminator $V_{thres.}$ values are reported in Table 2.2. Ideally the Discriminator values are set a few mV less than the SRS, but due to the small SRS voltage levels of -8.4 mV and the larger minimum $V_{Thres.}$ of -10 mV of the Model 710 Discriminator, ideal levels could not be achieved.

Fibre	1	2	3	4	5	6	7	8	Top	Bot.
SRS (mV)	-8.8	-8.4	-9.6	-6.8	-11.2	-14.8	-8.0	-8.0	-92	-84
$V_{thres.}$	-10.0	-9.9	-10.0	-10.0	-9.9	-10.0	-9.9	-10.0	-89.7	-82.7

Table 2.2: Measured smallest real signal (SRS) voltage and corresponding set Discriminator $V_{thres.}$. Ideally the Discriminator $V_{thres.}$ would be a few mV less than the measured SRS values, but the Phillips Scientific model 710 Discriminator [58] had a minimum $V_{thres.}$ of -10 mV. The uncertainty on the SRS fibre measurements was estimated to be ± 0.5 mV. The uncertainty on the $V_{thres.}$ measurements was ± 0.1 mV. On the plates, the uncertainty for SRS and $V_{thres.}$ are ± 1 mV and ± 0.1 mV respectively.

At this point, the Discriminator $V_{thres.}$ was set properly to maximize noise rejection while not vetoing real signals.

2.2.2 Appropriate Timing

The event trigger caused a ~ 55 ns delay between the Fan-out and the output of the final logic unit. To compensate for this delay raw signals needed to be delayed by 60-65 ns. A propagation speed of 1.94×10^8 m/s was measured in RG174 coaxial cables. In order to delay the signal by 60-65 ns, a $\sim$ 12 m cable was needed. All eight cables were made to have a propagation time of 62 ± 3 ns, to be sure that raw signals arrived at the ADC after the signal coming from the event trigger output arrived at the ADC gate.

2.2.3 Accidental Coincidences

When dealing with high particle flux, there is a possibility that accidental coincidences occur strictly due to the random nature of radioactive decay and cosmic rays. If the accidental coincidence rate R_{acc} is small it can be ignored, but it must first be estimated.

The R_{acc} for two events to occur simultaneously is directly related to the rate of both events individually (s_1, s_2) and the duration τ of both pulses (assuming the same time width for each pulse, and that "simultaneous" is defined as any timing overlap of the two signals), and is given by [22]:

$$R_{acc} = 2 s_1 s_2 \tau \tag{2.1}$$

However, since this experiment dealt with eight fibres, Equation 2.1 needed to be adapted to fit the situation. Each fibre was able to have an accidental coincidence with another (not counting twice) which leads to a $7+6+\cdots+1$ coefficient of Equation 2.1. If the average coincidence rate of each fibre is averaged to give s, Equation 2.1 becomes:

$$R_{acc,doubles} = 56s^2\tau \tag{2.2}$$

In general, to choose r fibre hits from n fibres, Equation 2.1 results in:

$$R_{acc} = 2\binom{n}{r}s^r\tau^{r-1} \tag{2.3}$$

Which is what was used to calculate accidental coincidence values in the multiplicity graphs throughout this chapter. The result from this investigation was that the accidental coincidence rate is not too low to be ignored, but the effect is very small. However, if higher rates and more fibres were used accidentals could become an issue.

Many calibration checks were made to ensure signals arrived at appropriate times and that $V_{Thres.}$ levels were set appropriately. A calculation has also been described to show that accidental coincidences had an effect (albeit small) on the results of this experiment. After the calibration was complete and the setup was functioning properly the experiment then proceeded into the preliminary results phase; but first, a description of data collection and analysis will be provided.

2.3 Data Collection and Analysis

2.3.1 Data Collection

A Unix based personal computer was used for data collection and was connected to a Computer Automated Measurement and Control (CAMAC) crate. The CAMAC crate is an electronic crate that is used as an old standard for data collection with CAMAC electronic modules. The computer was connected to the CAMAC via a Small Computer System Interface (SCSI) bus to enable high speed data transfers.

In the electronics setup, as shown in Figure 2.3, only two ADCs (g,h) and one Scaler (f) were read out by the computer. ADC (g) accepted input for the raw signals that came from the Fan-out module which replicated the raw PMT signals. ADC (h) accepted input from the Discriminator which sent digital signals indicating if a specific fibre was activated. The Scaler (f) kept track of the coincidence events for each individual fibre, and the total events for S1, S2, and SF.

The data collection program was written with the purpose of reading data from the ADCs and Scaler modules in the CAMAC crate, and writing the values to a file for analysis. When an event had occurred, a signal was sent to ADC (h) which was checked by the program. If ADC (h) indicated there was an event the program would pause signal collection (by sending a "veto" NIM signal to the NIM logic unit modules), then read out the information stored physically in the CAMAC modules, and write them to a file. A typical line found in this file is shown in Table 2.3. The coincidence event (Scaler) information for S1, S2 and SFs was written to a separate file.

ADC	ADC (h)							
Var.	D1	D2	D3	D4	D5	D6	D7	D8
Counts	1100	1100	65	71	65	66	69	67

Table 2.3: A typical data write-out from the data collection program. The second row represents the output variables, where D is a digital signal. The values in the Counts row is shown from an example data-run (collected on the September 1st, 2011). Note the two 1100 values represent a double coincidence. The values in row three are in units of 0.25 pC/count.

To ensure the 16 bit Scaler did not overflow in between being read and cleaned, the program would regularly read out the Scaler channel values and store them in internal program variables. Once the program was complete (that is, the data run ended), the counts stored in these variables (along with the test duration) were written to another file to be later used for analysis.

2.3.2 Data Analysis

A MATLAB code was made to read in data files and bin the data according to what type of coincidence occurred during each event. An example of the data written during an event is shown in Table 2.3, which shows an example of a double coincidence occurring. The different bins were: no coincidences, single, double, triple, up to octuple and non-adjacent double, non-adjacent triple, up to non-adjacent septuple. Finally, a bar graph was generated showing the number of counts in each bin. An example of the different bins, and the type of data that populates a particular bin, is shown in Table 2.4.

ADC	ADC (h)								Coinc. Type
Var.	D1	D2	D3	D4	D5	D6	D7	D8	
Counts	1100	1100	65	71	65	66	69	67	Double
Counts	70	70	63	1101	65	65	69	67	Single
Counts	71	67	1100	71	64	1100	69	67	NA-Double
Counts	1098	1098	1098	1098	1098	1098	1098	1098	Eight
Counts	69	65	1099	65	1099	65	66	1099	NA-Triple

Table 2.4: This table shows a few examples of different ADC values read out after an event occurred. The eight values were then sorted into bins depending on how many scintillating fibres were activated during each coincidence. These bins were later used to determine the cross-talk and multiplicity of the painted and unpainted trials.

One quantity that was also calculated by this program is the "multiplicity" of the fibre firings. This is a measure of the cross-talk occurring in an SFT due to all cross-talk and/or noise. Multiplicity (M) is defined as average number of fibre hits during the passage of a particle, divided by the expected number of hits [18]. For example, if a particle passed through a single layer scintillating fibre plane, the expected number of hits would be 1 (if the incoming particle beam is perpendicular to the plane). If two fibre channels were continuously activated during the passage of one particle, $M = 2$. Qualitatively, in the context of the measurements performed in the thesis, M is a measure of all the cross-talk effects in a SFT (and is later defined quantitatively in Equation 2.9). "It is essential to have low multiplicity which is close to 1 in order to obtain good tracking" [18]. Note that in applications of SFTs in high-rate environments, M is less a direct measure of cross-talk, and more a measure of the complications/difficulties associated with having multiple fibres getting hit within an event-coincidence time window.

The data collection program proved very robust and was able to be used for diagnostic purposes along with actual data collection. The MATLAB analysis program proved invaluable for this experiment and could be used again in the future as it was coded to be user friendly and accepts a number of different input file types with little effort. Now that an explanation of the file format has been given, preliminary results will be discussed.

2.4 Preliminary Results

Preliminary data trials were performed in order to work out problems with data collection and the experimental setup. This was the final diagnostic stage before actual experimental data was taken. This section will discuss preliminary results that were found, which resulted in adjusting and modifying the setup of the experiment. One issue was found with the placement of fibres on the face of the PMT that resulted in light leaking into adjacent channels at the face of the PMT where fibres were connected to the photocathode. Another issue with electronic noise was also encountered.

The analysis program output a bar graph comparing the number of single coincidences, adjacent double coincidences, triple coincidences, etc, and also showed the number of non-adjacent doubles, triples, etc. Adjacent and non-adjacent refer to the physical placement of the fibres. For example: If fibre one and two, which were physically adjacent to each other, were both activated within 50 ns of each other, the program incremented the "double coincidence" bin. Similarly, if fibres three and five, which are physically non-adjacent, were both activated within 50 ns of each other, the

program incremented the "non-adjacent double coincidence" bin. More coincidence situations exist, and some were shown in Table 2.4.

Electronic ringing in the signal cables was found during initial trials which caused a large number of octuple coincidences. Figure 2.4 shows a bar graph output from analysis of preliminary results. This graph shows the number of coincidences that simultaneously occurred during each data read out. The large number of octuple coincidences was not desired, as it indicated that cross-talk was occurring in the system that was most likely not due to light leaks. The signal was later viewed by the oscilloscope to confirm that light leakage was not the issue. The ringing was most likely due to sporadic capacitance effects of the light tight box that the test fibres and PMT were held in. These effects should be investigated in the future to improve the light tight enclosure.

Once the fibres signal cables were observed with the oscilloscope it was found that ringing was occurring between the PMT and before the signal arrived at the electronics. The only electronic elements that could have caused an issue were ECL adapters used to route 32-pin cables in and out of the light tight box. In an attempt to eliminate the noise, cables were routed directly from the PMT to the electronics. Re-routing the cables in this way eliminated the ringing, and reduced the number of octuple coincidences to zero.

After re-routing signal cables to bypass ECL adapters, an additional trial was executed to ensure the ringing was removed. Accidentally, fibre two's cable had been unplugged due to moving the light tight box to fix the ringing, and was not noticed until the test was complete. However, even though fibre two had no cable

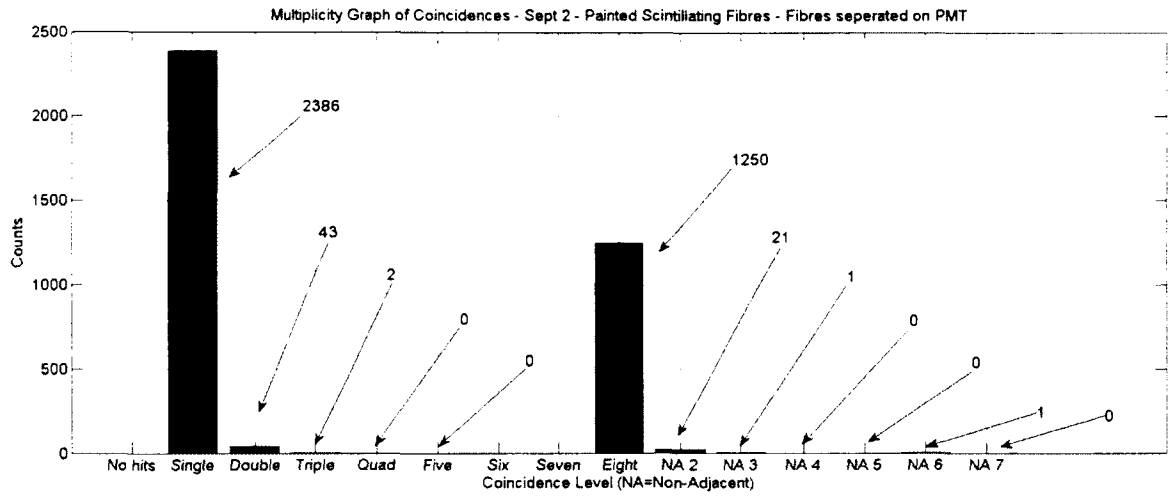

Figure 2.4: A bar graph output from analysis of preliminary results of the cross-talk experiment. This graph shows the cumulative number of different coincidence types that occurred. Note the unwanted number of octuple coincidences, which was the result of electronic noise in the signal cable that occurred sporadically, most likely due to capacitance effects of the light tight box that the test fibres and PMT were held in.

attached to it, there were still 261 counts present. The counts for each fibre from this data-taking run is shown in Table 2.5. The large difference in counts arises from the placement of radioactive sources above the fibres, since many individual sources were placed on top of S1 to increase the even rate as much as possible.

A test was subsequently performed operating under the assumption that the noise in fibre two was electronic in nature. All signal cables were disconnected and after an 18 hour data collection period, only 35 counts in total were found in total between all eight fibres. This should have been zero, but in lieu of what was previously found from fibre two, a much better result. This lead to the belief that the

Fibre	1	2	3	4	5	6	7	8
Counts ($\times 10^4$)	13	0.0261	32	7.2	5.1	49	4.1	9.8

Table 2.5: This table shows the counts for each of the eight scintillating fibres during the September 17th, 2011 preliminary trial. Fibre 2 was accidentally unplugged before testing, however, there were still counts appearing, but the total is very small ($< 0.6\%$) compared to the other properly-connected fibres. This was most likely due to electronic noise. The difference in counts between fibres arises from the placement of radioactive sources. Noticing the counts in the second channel, which should have been zero, lead to investigating the origin of the 261 counts.

noise was caused by true equipment cross-talk. More specifically, that when a signal was going through a module, there was some signal leakage into another channel. In order to eliminate this noise, $V_{Thres.}$ of the Discriminator was increased to -15 mV for all channels. This test resulted in zero counts and the noise problem was eliminated.

Another important phenomenon that was revealed from preliminary tests was light leakage at the face of the PMT. Since fibres did not have perfect contact with the PMT some light was able to leak out. This light may have spread to nearby PMT pixels, leading to false signals in those channels. This was determined from testing the signals in adjacent rows (empty) to where fibres were placed on the PMT face.

Initially, fibres were lined up and inserted into row four of the PMT. The electronics were connected to the channels one row above fibres. In reality, no fibres were connected to the read-out channels. This should have resulted in zero counts in all of those pixels; however, 523 singles, four doubles, five non-adjacent doubles and

one non-adjacent triple were found. At this point, it was believed that photons were leaking into nearby pixels due to cross-talk at the face of the PMT.

It was expected that increasing the distance between fibre pixels and read-out pixels would decrease the photons arriving at the read-out pixels. The next test was performed under the same test conditions, except that the analysed pixels were two rows above the fibre input pixel row. Again, no fibres were physically attached to these channels. In that case, as expected, the number of coincidences was decreased. The results showed 145 singles, two doubles, five non-adjacent doubles, two triples and one quad.

After identifying this problem, the fibres were separated to maximum spacing on the PMT face. Even if the problem was not completely eliminated, it was minimized with the equipment that was available. The final configuration of fibre placement is shown in Figure 2.2 in the right panel.

The preliminary tests and results have shed light on some important phenomenon that should be later investigated. However, for the purpose of this thesis, the problems were identified and corrected. In the case of electronics noise, the problem was almost completely eliminated. With the issue of fibre separation on the PMT, in order to minimize the problem, the fibres were separated as much as possible. These corrections allowed the experiment to proceed to the next phase of real data collection and analysis of results.

2.5 Results of Cross-Talk Experiments

The results and analysis of this experiment, and whether or not the results are consistent with the hypothesis, will be presented. Before showing those results, information about painting fibres for the painted portion of the experiment will be discussed.

2.5.1 Painting Scintillating Fibres

Scintillating fibres were painted in order to see if painting reduced the cross-talk between adjacent scintillating fibres. To determine a good painting method and which paint to use, three different methods were tested qualitatively. Different types of coatings are discussed in Section 1.6.1, however, only two types of paints were investigated.

Setup and Results for paint tests are shown here. Trial:

1.
   - Test: Eight scintillating fibres were separated and hung from a rack then sprayed with Krylon-Fusion Spray Paint for Plastic.
   - Result: Paint adhered to fibres. Fibres were slightly bent, most likely because their ends were lying on the table, and not from the paint drying.
   - Note: Painting was quick and easy once fibres were hung.

2.
   - Test: A bundle of fibres were laid out side by side and painted with Rust Paint using a paint brush. They were then hung up together to dry.
   - Result: After drying, fibres clumped together due to the paint bonding together. The paint also caused fibres to bend a significant amount, and

attempting to straighten them after paint was dried resulted in paint cracking and chipping.

- Note: Painting was difficult and messy.

3.
- Test: Fibres were spray painted with trial 1 paint (Krylon-Fusion Spray Paint for Plastic), however, were grouped together rather than being separated. Fibres were hung to dry.
- Result: Fibres clumped and bonded together.
- Note: It was easier to spray paint fibres than paint with a brush.

In conclusion, spraying fibres (as in trial 1) with Krylon-Fusion Spray Paint for Plastic provided the quickest and easiest method to paint fibres, along with having the best quality results. Fibres were evenly painted, and were barely bent after drying. This paint also did not crack and chip while being moved around after dried. This painting method (trial 1) was used to coat the fibres used during the cross-talk experiment.

2.5.2 Effects of Increasing Discriminator $V_{Thres.}$

Increasing the $V_{Thres.}$ should result in a decrease in the number of real signals entering the electronics - that is why the smallest real signal was measured, in order to optimize $V_{Thres.}$ relative to the smallest signal. However, if electronic cross-talk becomes a problem it may be desirable to increase $V_{Thres.}$ at the cost of losing real signals (as was already discussed in Section 2.4. This effect was briefly investigated further by increasing $V_{Thres.}$ to -20 mV.

The experimental parameters for the $V_{Thres.} = -20$ mV test with painted fibres (Test 1) was the same as the $V_{Thres.} = -15$ mV test with painted fibres (Test 2), except for the test duration. Test 2 lasted 66 hours, while the Test 1 lasted 18 hours.

In 18 hours, Test 1 (higher threshold) had $N_1 = 159$ single counts, where in 66 hours of Test 2 (lower threshold) had $N_2 = 1503$ singles. If Test 2 is normalized to Test 1's duration, then $\frac{18}{66} \times 1503 = 410$ counts. The uncertainty in each of these counts is $\sqrt{N}$ where N is the number of counts. This means $\sigma_{N_1} = \sqrt{N_1} = \sqrt{159} = 13$ and $\sigma_{N_2} = \sqrt{N_2} = \sqrt{410} = 20$. Comparing the two values (counting singles only), with uncertainties:

$$N_1 \pm \sigma_{N_1} = 159 \pm 13 \text{ counts}$$

$$N_2 \pm \sigma_{N_2} = 410 \pm 20 \text{ counts}$$

Shows the two counts (this can easily be expressed as rates as well) are significantly different. Thus by increasing the Discriminator $V_{Thres.}$ by even a few mV to decrease cross-talk causes the number of real signals entering the electronics to be drastically reduced.

2.6 Uncertainty Analysis: Cross-talk

An analysis must be performed on the data collected from the painted and unpainted cross-talk experiments in order to determine the uncertainty in the measure-

ments, and to see if the two values are experimentally different.

The uncertainty analysis is completely statistical because systematic uncertainty in the detector setup is negligible (and, at least, is the same for both painted and unpainted fibres). The main equipment uncertainty is negligible and ignored since the number of events is quite low, leading to large/dominant statistical uncertainties. Two final values were calculated in this experiment: (1) the percent cross-talk reduction after after applying paint, and (2) the multiplicities of a single layer particle tracker with and without paint.

2.6.1 Percent Cross-talk Reduction

To determine the percent cross-talk reduction (ΔC), the unpainted cross-talk ($C_{unpainted}$) and painted cross-talk ($C_{painted}$) were calculated. A good measure of cross-talk occurring in our single-layer test version of an SFT is the ratio of the number of multiple coincidences (n_m) to number of single fibre hits (n_1) after the passage of many particles. However, since the number of accidental detections (n_{acc}) was comparable to the number of multiples recorded $n_{multiples\ recorded}$, it must be accounted for. This is taken care of by subtracting n_{acc} from the number of recorded multiples leading to:

$$n_m = n_{multiples\ recorded} - n_{acc} \tag{2.4}$$

which leaves the cross-talk as:

$$C = \frac{n_m}{n_1} \tag{2.5}$$

The general uncertainty propagation formula was used to determine the uncertainty in Equation 2.5 [64, 65], which for an arbitrary function $q(x, ..., z)$ is:

$$\sigma_q^2 = \left(\frac{\partial q}{\partial x}\sigma_x\right)^2 + \cdots + \left(\frac{\partial q}{\partial z}\sigma_z\right)^2 \tag{2.6}$$

Where σ_x is the uncertainty in the variable x. Applying Equation 2.6 to 2.4 yields:

$$\sigma_{n_m}^2 = \sigma_{n_{multiples\ recorded}}^2 + \sigma_{n_{acc}}^2 \tag{2.7}$$

where $\sigma_{n_{acc}}$ equals $\sqrt{n_{acc}}$. Now applying Equation 2.6 to 2.5 yields:

$$\sigma_C^2 = \left(\frac{1}{n_1^2}\sigma_{n_m}\right)^2 + \left(\frac{n_m^2}{n_1^4}\sigma_{n_1}\right)^2 \tag{2.8}$$

Equation 2.5 and 2.8 will be used to calculate the value of the cross-talk and its uncertainty.

2.6.2 Multiplicity

Another way to represent the amount of cross-talk is using the "Multiplicity". Multiplicity (M) was presented in Section 2.3.2 and is defined as the average number of fibre hits during the passage of a particle divided by the expected number of hits [18]. M can be calculated from the information collected during this experiment by:

$$M = \sum_{i=1}^{8} \frac{in_i}{N} = \frac{n_1 + 2n_2 + \cdots + 8n_8}{N} \tag{2.9}$$

where n_1 is the number of single coincidences, n_2 is the number of doubles, up to n_8 the number of octuples and N is the total number of coincidences. To determine the uncertainty for Expression 2.9, Equation 2.6 is applied.

$$\sigma_M^2 = \left(\frac{1}{N}\sigma_{n_1}\right)^2 + \left(\frac{2}{N}\sigma_{n_2}\right)^2 + \cdots + \left(\frac{8}{N}\sigma_{n_8}\right)^2 + \left(\frac{n_1 + 2n_2 + \cdots + 8n_8}{N^2}\sigma_N\right)^2 \quad (2.10)$$

Again here, as in Equation 2.7, the number of accidentals must be subtracted from each value, and the uncertainties added in quadrature.

2.6.3 Result of Unpainted Fibres

The final result shown below in Figure 2.5 was attained by passing ionizing particles through scintillating fibres. Observations were made to see if one or more fibres were simultaneously activated during one particle's pass. Unpainted, or uncoated, fibres had the potential to leak scintillation light produced inside one fibre into adjacent fibres. This would give rise to double and triple coincidences, etc.

The top number attached to the arrows pointing to the bins are the number of counts of a certain event type that occured during the experiment. The bottom number is the expected n_{acc} if no cross-talk effects existed, as discussed in Section 2.2.3.

The multiplicity of the unpainted fibres of $M_{unpainted} = 1.027 \pm 0.071$, which was calculated using Equations 2.9 and 2.10. This number is equivalent to the ideal multiplicity of 1 within uncertainty, which would indicate only one fibre being activated during the passage of a particle. The low multiple-to-single ratio of

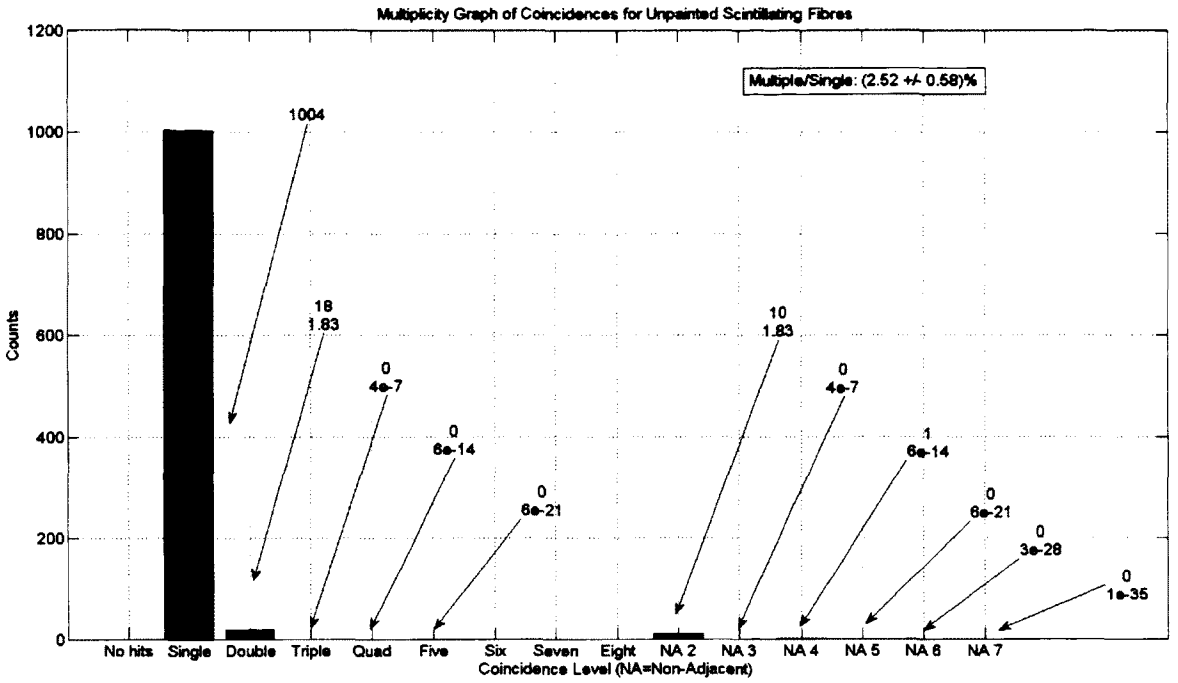

Figure 2.5: The results of a 66 hour test for the unpainted adjacent scintillating-to-scintillating fibre cross-talk experiment. This test was performed with a Discriminator $V_{thres.}$ of -15 mV. The top number at the ends of arrows are the number of coincidences of a certain type, the second number is the expected number of accidental counts n_{acc} if no cross-talk exists. This data was collected on September 26th, 2011.

$C_{unpainted} = (2.52 \pm 0.58)\%$ for the unpainted fibres shows that for $V_{Thres.} = -15$ mV only this small amount of cross-talk exists.

2.7 Result of Painted Fibres

It was expected that painting fibres would reduce the multiplicity and cross-talk of a scintillating fibre setup. In principle, a reduction in cross-talk between adja-

cent scintillating fibres would be caused by lowering the leakage of scintillation photons from an activated fibre. Under the same test conditions as the unpainted test. the results of the painted fibre experiment are shown in Figure 2.6. This experiment had a multiplicity of $M_{painted} = 1.007 \pm 0.039$ and a multiple-to-single ratio of $C_{painted} = (0.63 \pm 0.25)\%$. The value for $C_{painted}$ was significantly lower thn $C_{unpainted}$,

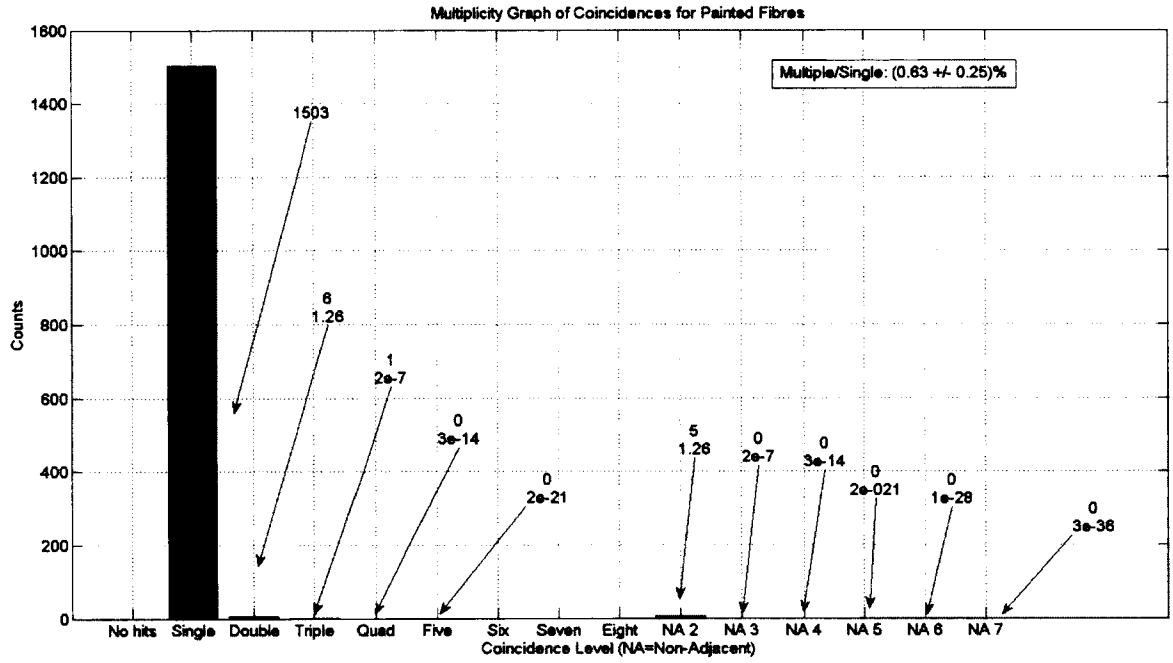

Figure 2.6: The results of a 66 hour test for the painted adjacent scintillating-to-scintillating fibre cross-talk experiment. This test was performed with a Discriminator $V_{thres.}$ of -15 mV. The top number at the ends of arrows are the number of coincidences of a certain type, the second number is the expected number of accidental counts n_{acc} if no cross-talk exists. This data was collected on September 23rd, 2011.

which indicates that painting scintillating fibres does reduce adjacent scintillating-to-

scintillating fibre cross-talk.

One more step was taken to illustrate the reduction in cross-talk. Applying the uncertainty propagation Equation 2.6 to $\Delta C = C_{unpainted} - C_{painted}$ simply results in adding the uncertainties in quadrature; therefore, the percent cross-talk reduction ΔC is:

$$\Delta C = (1.89 \pm 0.63)\% \tag{2.11}$$

This result is very conclusive, showing that within statistical experimental uncertainty the cross-talk occurring can be reduced by coating fibres with a light absorbent paint.

It is also important to understand the Confidence Interval of knowing that painting fibres reduces cross-talk. Since the result in Equation 2.14 is accurate in stating that painting fibres reduces cross-talk to within $n_\sigma = 3\sigma$, the confidence interval can be calculated using:

$$CI = 100 \cdot \mathrm{erf}\left(\frac{n_\sigma}{\sqrt{2}}\right) = 99.73\% \tag{2.12}$$

This very high level of confidence level indicates that the result is conclusive. Stating this result another way: It is known with 99.73% confidence that painting fibres reduces cross-talk between adjacent scintillating fibres by a measurable amount.

As discussed in Section 2.2.3, another way of looking at the effects of fibre coating is by calculating the charged particle multiplicity of the detector.

Using the values found in Figure 2.5 and 2.6, $M_{unpainted}$ and $M_{painted}$ were

calculated to be:

$$M_{unpainted} = (1.027 \pm 0.071)\% \qquad M_{painted} = (1.007 \pm 0.039)\% \tag{2.13}$$

Unfortunately, the calculated values for $M_{unpainted}$ and $M_{painted}$ in Equation 2.13 are the same within experimental uncertainty and no conclusions can be drawn about the effects of coating fibres on multiplicity. It cannot be said that painting fibres has no effect on multiplicity, because the uncertainty also includes the lowest possible limit of $M = 1$ for both the values of $M_{unpainted}$ and $M_{painted}$. Therefore, no conclusions can be made from this calculation; this indicates the above ΔC method of comparing cross-talk is a more sensitive measurement quantity.

2.8 Conclusion: Cross-talk

The analysis of the results for the cross-talk experiment performed during this thesis shows that coating scintillating fibres with light absorbent black paint reduces the adjacent scintillating-to-scintillating fibre cross-talk by:

$$\Delta C = (1.83 \pm 0.63)\% \tag{2.14}$$

This result is certain even with large statistical uncertainties and is reproducible under the described experimental conditions. Further, this indicates that it is known with a 99.73% Confidence Interval that painting fibres reduces cross-talk by a measurable amount.

Chapter 3

Different Fibre-end Finishes and Optical Couplants in Combination and Their Effects on Light Transmission

This chapter describes an experiment on different fibre-end finishes in combination with different fibre couplants and their effects on light transmission. This is being investigated to address the questions: (1) which optical couplant, and (2) what fibre-end finish, provides the best light transmission efficiency. These two questions have been combined into one experiment. It is desired to have light transmission maximized in order to achieve the strongest signal possible before it enters the analysing electronics. Another key reason is to have the signal as large as possible compared to electronic noise in order to reduce the effects of noise on the analysis of experiments.

As mentioned in Section 1.6.2, a number of different optical couplants are commonly used. In decreasing popularity, these include: optical epoxy, optical grease, mineral oil, silicon connectors, UV curing glue, and air. Because of budgetary and time restrictions, not all optical couplants could be investigated for this thesis, so the two most common and the simplest, optical epoxy, grease and air have been tested.

On the same note, a number of different fibre-end finishes exist, as discussed in Section 1.6.3. The different finishes include: scissor cut, sanded, polished, annealed, and factory finish. These finishes have all been investigated qualitatively, while sanded, polished, annealed and factory finishes have been investigated quantitatively.

It has been hypothesised that a smooth fibre-end finish coupled with optical epoxy will result in the largest light transmission.

The experimental setup, results, analysis and conclusion will be presented in this chapter.

3.1 Experimental Setup: Light Transmission

This section will describe the setup needed in order to retrieve information about light transmission while minimizing uncertainties (and keeping the budget reasonable).

The setup consisted of eight sets of fibres. Each set included five test scintillating fibres optically coupled to five test light guides, and three control light guides. At the non-coupled end of the scintillating fibres, there was a system of blue LEDs (as shown in Figure 3.1) used to light the fibres. The LED pulsed with a

duration of 210 ± 5 ns and a pulse-separation period of 150 ± 2 μs, which was constant throughout all tests. The control light guides were needed to account for any possible fluctuations in the LED's intensity and/or in the overall gain of the PMT. Five test fibres were used in order to be able to provide "repeated measurements" for the particular test combination, since in every trial the five scintillating fibres and five light guides had the same fibre-end finish and optical couplant. The fibre-end finish being investigated in each case was applied to one end of the scintillating fibres and to the light guide end.

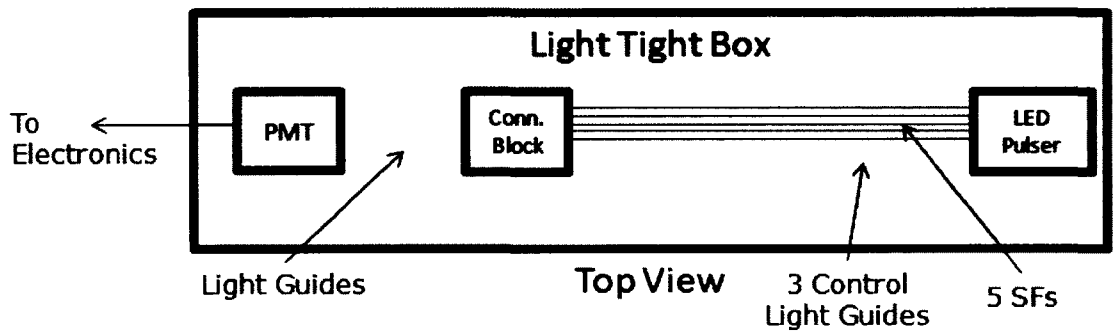

Figure 3.1: This Figure shows the experimental setup of the light transmission experiment. A blue light LED pulser sent photons into five scintillating fibres and three control light guides. The photons in the scintillating fibres encountered an optical couplant and light guide at the connection block junction, where some signal was lost. The photons were then transmitted into light guides and routed to the PMT where signals were collected. All this occurred inside a light tight box.

Three holding blocks with holes for fibres were designed and machined to precisely hold fibres in place. The PMT connection block (PCB) was used to connect

and hold fibres to the PMT face[1]. The fibre connection block (FCB) was used to connect scintillating fibres to light guides, and the light connection block (LCB) was used to feed the LED light into the fibres. Figure 3.1 indicates the locations of the three connection blocks. The connection blocks were used to hold fibres securely in place so that nudging or vibrations had little effect on the optical interface.

The PMT was used to collect signals from the light guides, which were all of the same type and same diameter. The fibres and PMT are an important part of the experiment and are discussed in the next section.

3.1.1 Fibres and PMT

In the light transmission experiment, the scintillating fibres, light guides, and optical couplants were the main materials being tested. Only 0.5 m long, 1 mm diameter BCF-20 [49] scintillating fibres were used throughout the whole experiment. There were two different lengths of 1 mm diameter BCF-68 [49] light guides used: 0.7 m for the control light guides, and 0.2 m for the test light guides.

The light guides were connected at one end to an H7546B PMT which was described in Section 2.1.1. The fibre placement on PMT pixels is similar to the previous experiment, reported in Chapter 2. Figure 3.2 shows the fibre to PMT pixel connection location on the PMT face; this configuration provided maximum fibre separation in order to reduce PMT face cross-talk as much as possible. The PCB was machined to hold fibres in place directly over the pixels shown in the Figure.

Two different optical couplants were used in this experiment to couple

[1]This is a "cookie" as discussed in Section 1.5.2.

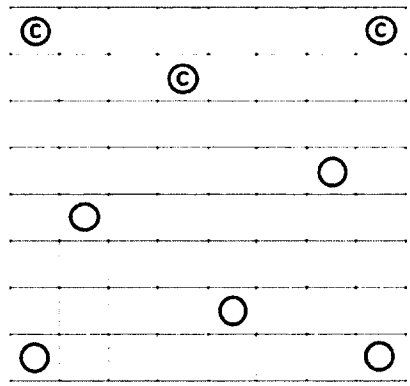

Figure 3.2: This Figure shows light guide and control light guide input locations on the PMT face. This configuration maximized fibre separation and minimized PMT face cross-talk. The fibres with a "c" on them represent the placement of control fibres.

scintillating fibres to light guides. Dow Corning 20-057 optical coupling compound (grease) and type EJ-500 optical epoxy were the two couplants chosen (if a larger budget was available, others would have been tested as well). This choice was motivated by the popularity of the two, and because previous studies suggested the two couplants had high light transmission of 95% [27] and 98% [43] for optical epoxy and grease, respectively.

Once the photons arrived at the PMT, the light was collected and converted into an electronic signal. The signal was then processed by the high-speed electronics.

3.1.2 Read-out Electronics

The electronics for this experiment needed to be able to provide the computer program with values that were proportional to the intensity of light that passed

through the optical couplant interface. This was accomplished by using ADCs to determine the signal strength and reading out values stored inside the ADC every time an LED pulse finished. The electronics setup is shown in Figure 3.3.

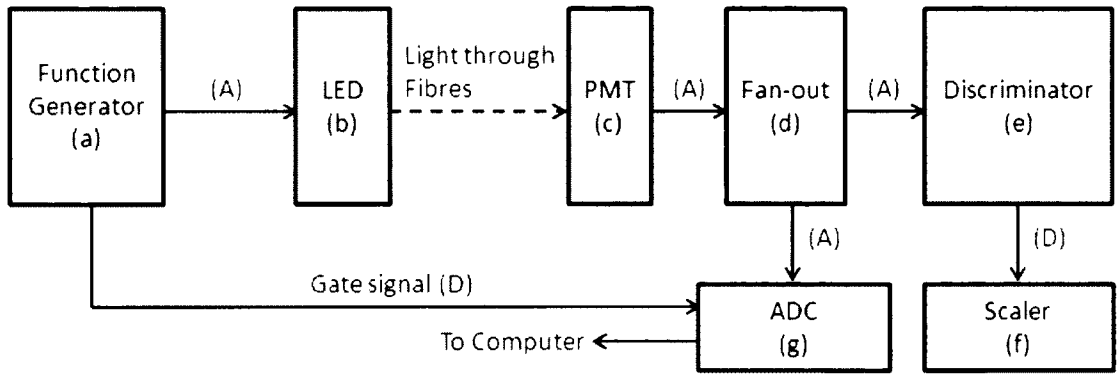

Figure 3.3: This Figure shows the electronics setup of the light transmission experiment. A function generator (a) was used to generator waveforms which were sent to an LED (b) and ADC gate (g). The LED emitted light that travelled to a PMT (c), which converted the photons into an electronic pulse that was sent to: (1) the ADC (g) to be processed and (2) a Fan-out (d). The Fan-out (d) replicated the raw input signals and sent them to a Discriminator (e) which converted signals from analog to digital. The digital signals were finally sent to the Scaler (f) for counting. The ADC (g) and Scaler (f) were read out by a computer.

A Berkeley Nucleonics Model 8010 Pulse Generator [66] was used to generate square waveforms which were sent to activate an LED, and to open the ADC gate to allow charge collection from the PMT signals.

The LED was designed in order to produce uniform light on one side to ensure all eight fibre ends received the same light intensity. Five LEDs were individ-

ually placed inside optical diffusers to help disperse the light isotropically. The LEDs and diffusers were then inserted into a Styrofoam block and evenly spaced, again, to aid in the dispersion of light. The front of the block, where the fibres were placed, was covered with translucent chemistry weigh-plates to provide a final stage of light dispersion.

When the LED was on, a pulse of light was sent down the scintillating fibres and control light guides, through the fibre-ends and optical couplant, then arrived at the PMT. The PMT converted the photons to a signal and sent all eight channels to a Fan-out module [57]. The Fan-out sent the duplicated signals to a Discriminator module [58] to be converted to a digital signal for counting in the Scaler module [61].

A signal was also sent from the pulse generator to the ADC gate input. This allowed charge collection from the signals sent to the ADC [59], which were also routed from the Fan-out.

In order for electronics to function properly and to account for any unexpected experimental issues, calibration and preliminary tests needed to be performed.

3.1.3 Calibration

Many calibrations needed to be performed in order to optimize settings and to allow for data normalization.

Since the scintillating fibres were physically being lit by an external light source, the electronic signals produced from the PMTs were large (in comparison to signals from passing MIPs). This resulted in large signals arriving at the Discriminator, so it was not necessary to determine the SRS.

ADC Calibration

ADC spectra were made for all ADC inputs to determine if the ADC was functioning properly. An example ADC spectrum from a radioactive β-source incident on Fibre 1 is shown in Figure 3.4. If a counter chip in the ADC module was broken, that particular bit would never be counted, and would be manifest in the spectrum by an ADC channel (x axis bin) being empty. An example of this is shown in Figure 3.5.

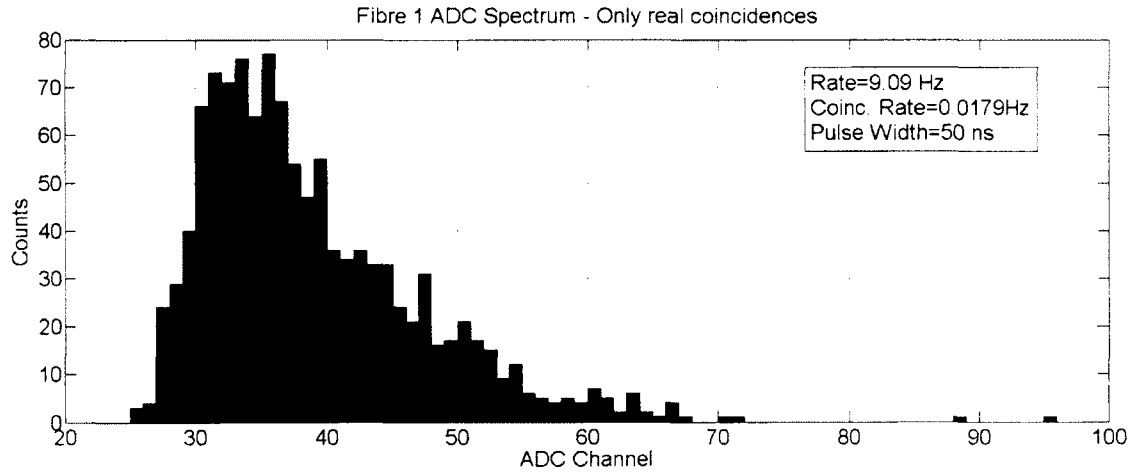

Figure 3.4: An ADC spectrum of a scintillating fibre being activated by radioactive sources and cosmic rays. This graph is a Poisson shaped curve which reflects the beta decay energy distribution.

Electronic noise levels can be found by determining the ADC pedestal. The pedestal is an output count from the ADC even when there is no true signal present. It can be determined by unplugging all inputs to the ADC and looking at the resulting spectra. An ADC pedestal analysis was done, and the histogram is

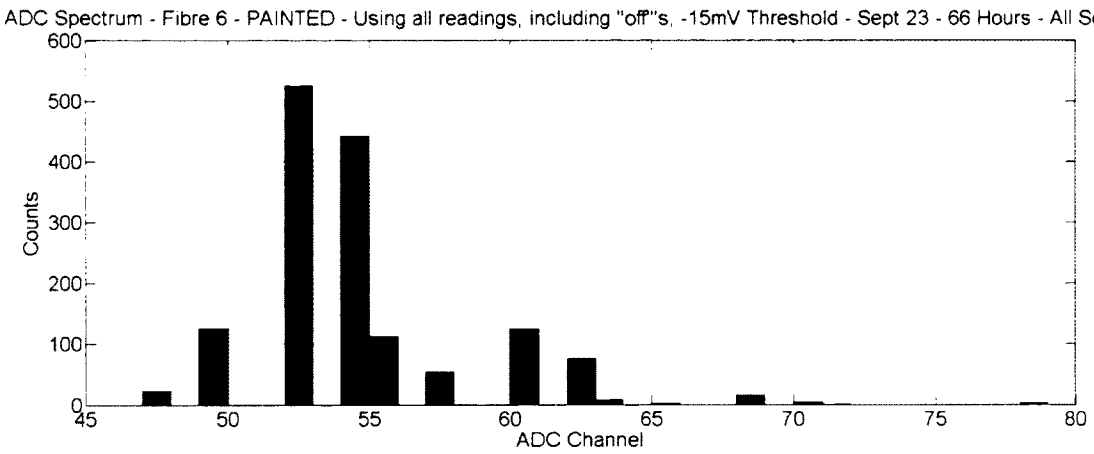

Figure 3.5: An example of a malfunctioning ADC. This spectrum should look similar to Figure 3.4. If a spectrum contains many counts across a continuous energy distribution, it is very improbable that specific bins will not fill up, as seen here. This malfunction is due to defective counting chips in the ADC.

shown in Figure 3.6. The ADC pedestal value must be subtracted off the ADC value to be used in data analysis. Additionally, even if no electronic noise was present, an ADC would still have a pedestal due to a built-in DC offset, and is proportional to the gate duration according to $1+0.003w$, where w is the gate width in nanoseconds [22].

After determining that all ADC inputs were functioning properly, a calibration for the PMT fibre holding block was performed.

PMT Connection Block (PCB) Calibration

PCBs were designed and machined to precisely place, hold, and align fibres to specific pixels on the PMT face. Although precise drilling was done, it was important to account for minor changes in the fibre's position. This was accomplished by

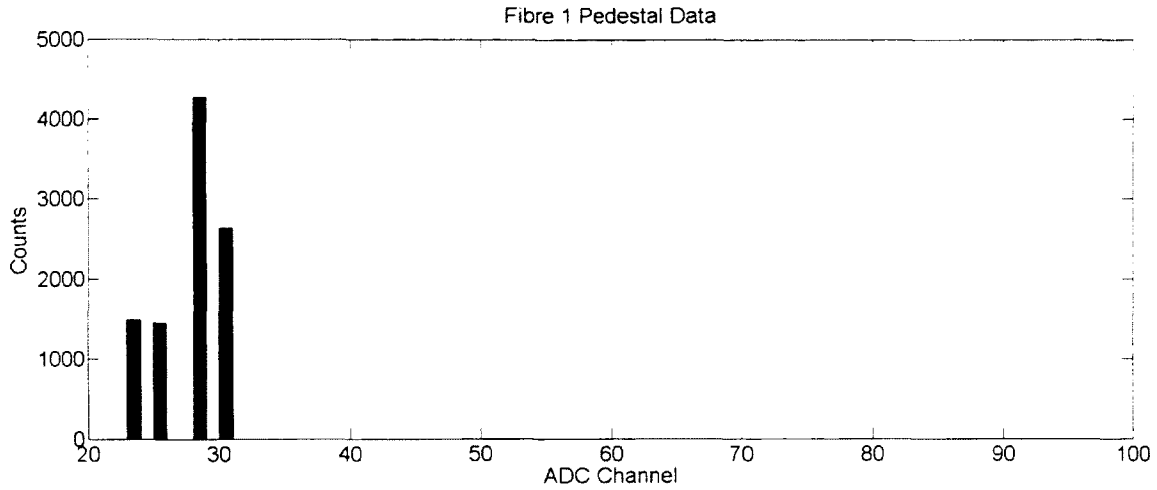

Figure 3.6: This Figure demonstrates an ADC pedestal. Even when no input wires are connected to the ADC, there is still some level of internal noise.

collecting information about the strength of signals over a range of fibre placements.

Eight different PCBs were built, and each had slightly different positioning of fibre holes. In addition, when the PCB was connected to the PMT, there was room for movement in the relative orientation. This calibration accounted for the uncertainty in fibre's position on the PMT face.

During actual testing conditions, a PCB was placed on the PMT face and secured for one test; it would then be removed, and another PCB would be attached for the next test. In an effort to account for the placement uncertainty associated with how the fibres aligned with its corresponding PMT pixel, 100 measurements were made for each PCB. In between each measurement (for each PCB), the PCB was removed and reattached to simulate the uncertainty in the position of the PCB when attached for the on/real test of a particular combination of fibre-end finish and

couplant. Slight changes in the position of the PCB led to measurable differences in the signal strengths measured by the ADC.

The important quantity for the actual experiment was the ratio of signal strengths of each individual fibre to the average of the control strengths. Because of this, calibration data was also divided by the average of the controls. Due to time constraints, only 100 measurements were able to be made for each PCB. This meant that there was barely enough data for a statistical treatment of the ratios. However, the ratio was assumed to be Gaussian with a well defined mean. From the 100 measurements, a calibration ratio mean (c_i) and standard deviation (σ_{c_i}) was calculated for each fibre hole i, in each PCB. σ_{c_i} was later used as the major source of uncertainty for the final experiment result.

Once this calibration data was collected, it was stored in calibration files later used to normalize the actual test data and to provide a measure of uncertainty. The normalization is accomplished because the same amount of input source light was transmitted to each PMT pixel used in testing in an identical fashion; since there were always 3 fibres (or pixels) used as a control group throughout the experiments to follow, the normalized response of any of the test pixels will be the measured response multiplied by the ratio of that pixel's mean response here divided by the average mean response of the three control fibres (this ratio is the c_i indicated above). With calibrations completed the experiment was ready for physics data collection.

3.2 Preparing Scintillating Fibres

The main goal of this experiment was to determine which optical couplants and fibre-end finishes had the best optical transmission. A secondary goal was to attempt to find a quick and easy way to finish fibres, while maintaining a high light transmission. The simplicity of finishing fibres is key, since typically $10^4 - 10^5$ fibres are used in an SFT. Long, complicated finishing techniques require many hours of work, and the more labour that goes into finishing a fibre, the more difference there could be in the ends of different fibres in an SFT. All finishes were applied to both the scintillating fibres and the connecting light guides.

In order to view fibre-end finish quality, pictures were taken using a Scanning Electron Microscope (SEM). A brief description of the finishing process is now given:

Factory Finish: With the secondary goal in mind, all fibre finishes were kept as simple as possible so the finish could easily be replicated and used on a large scale. The simplest fibre-end finish is clearly the finish the fibre supply company provides. These tests were done with no additional treatment to fibres. SEM images of factory fibre-end finished scintillating fibres are shown in Figure 3.7.

Sandpaper: In order to finish fibres with a sandpaper, they were first cut with fibre optic cutting scissors. Fibres were then hand held during sanding, and were pressed lightly against the sandpaper and moved in a circular pattern for ten seconds. SEM images of fine and coarse fibre-end finished scintillating fibres are shown in Figure 3.8 and 3.9 respectively.

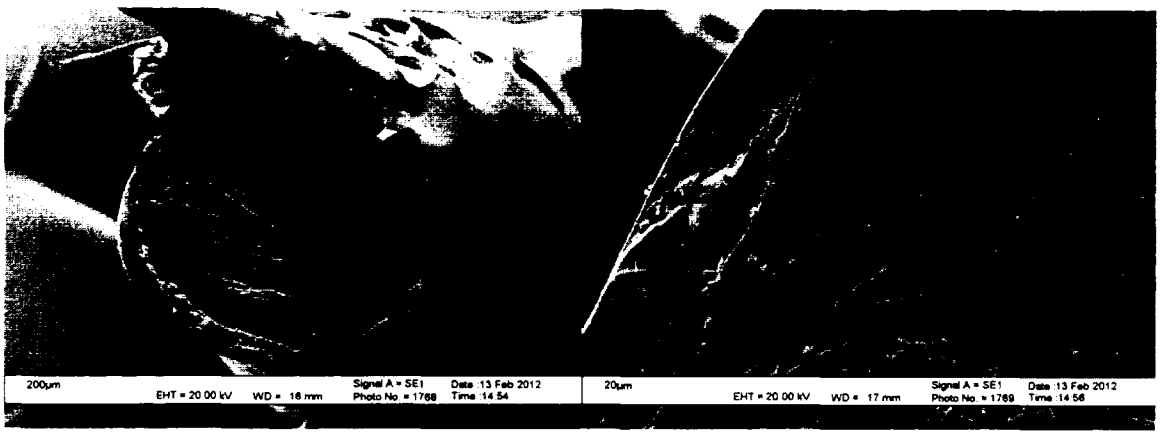

Figure 3.7: **Factory Finish** - SEM photographs of a factory scintillating fibre-end. The left panel shows the entire fibre face while the right panel is zoomed in. Note the PMMA cladding around the outside of the fibre in the right panel. Image parameters are reported on the photograph.

Figure 3.8: **Fine Sandpaper Finish** - SEM photographs of a 320 grit sanded scintillating fibre-end. The left panel shows the entire fibre face while the right panel is zoomed in. Note the PMMA cladding around the outside of the fibre in the right panel. Image parameters are reported on the photograph. The average granule size for 320 grit sandpaper is 36 μm

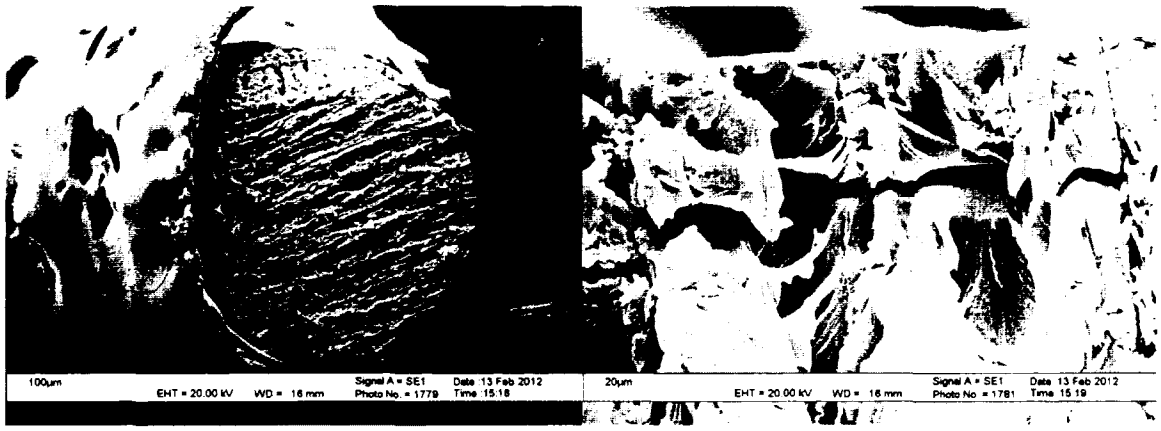

Figure 3.9: **Coarse Sandpaper Finish** - SEM photographs of a 40D grit sanded scintillating fibre-end. The left panel shows the entire fibre face while the right panel is zoomed in. Note the PMMA cladding around the outside of the fibre in the right panel. Image parameters are reported on the photograph. The average granule size for 40D grit sandpaper is 425 μm

Polish: Fibres were cut, then sanded as described above. Polish was then applied to a cloth fastened to a rotating motor. The fibre was pressed gently against the rotating cloth for ten seconds. The polish-filled cloth was then replaced with a clean dry cloth that the fibres were gently pushed against for ten seconds while the motor was rotating. Fibres were visually inspected to confirm all polish was removed, and if the polish was not removed, the cleaning step was repeated. SEM images of polished fibre-ends are shown in Figure 3.10.

Scissor Cut: A scissor cut finish was not directly tested, rather the fibre was annealed after being cut. Annealing is discussed in the next section. In order to cut fibres, a special pair of fibre optic cutting scissors were used. Sometimes this process

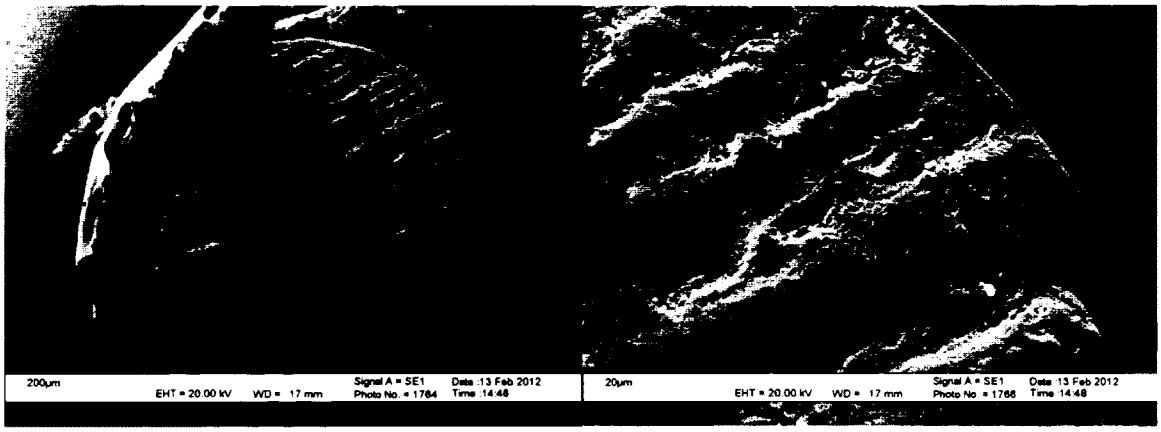

Figure 3.10: **Polished Finish** - SEM photographs of a polished scintillating fibre-end. The left panel shows the entire fibre face while the right panel is zoomed in. Note the PMMA cladding around the outside of the fibre in the right panel. Image parameters are reported on the photograph.

split the fibre in the center as is seen in SEM Figure 3.11.

The annealed finish procedure was much more complex, and will now be discussed at length.

3.3 Annealing of Fibres

A novel technique to finishing scintillating fibres and light guides has been developed and tested. This method involves heating fibre ends to a temperature above their glass transition temperature, then momentarily raising the temperature above their melting point, then quickly cooling them. Ideally, this would take a coarsely finished fibre and smooth it out.

This method could be adapted to a large scale fibre-end finishing project

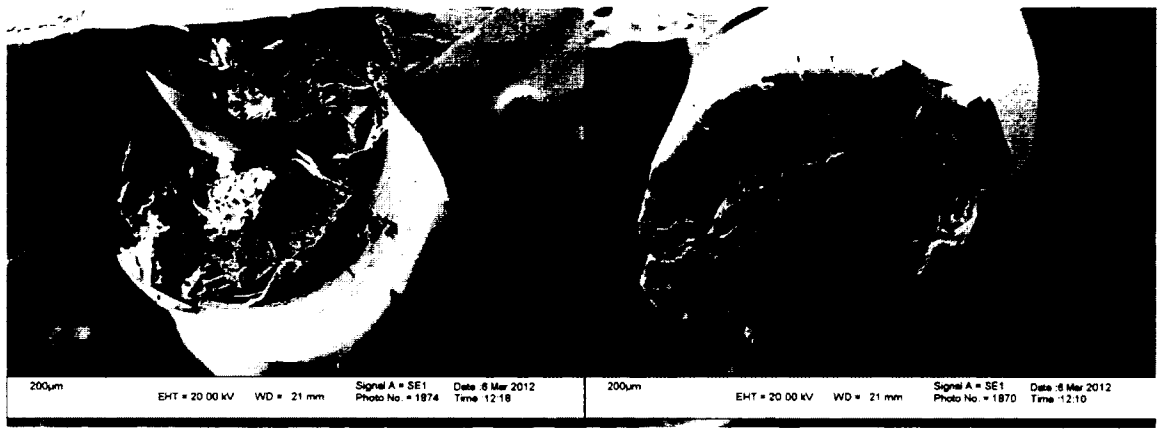

Figure 3.11: **Scissor Cut** - SEM photographs of a scissor cut scintillating fibre-end. The left panel shows a fibre that is split down the middle. The right panel shows a non-split fibre face. Note the PMMA cladding that is stretched down over the fibre face in the right panel. Image parameters are reported on the photograph.

with more development. However, for the purpose of this thesis, only the light transmission effects were studied, so the annealing setup was only designed to heat one fibre at a time.

3.3.1 Annealing Setup

The heating setup involved designing a holding apparatus to secure one fibre while its end was being heated, as shown in Figure 3.12. Heating was accomplished with a heat gun, capable of 400°C temperatures. The heat gun also had an adjustable rheostat and air flow input valve to regulate heat output.

Once the fibre was finished, it was then annealed according to the temperature profile in Figure 3.13. This temperature profile was followed because the material that makes up the core of fibres, PS, has a glass transition temperature of

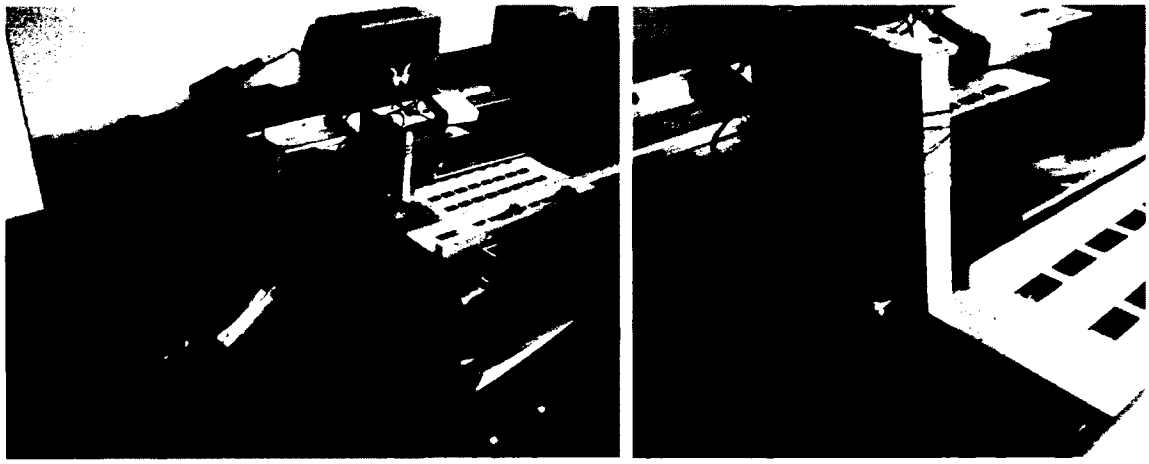

Figure 3.12: The figure shows the setup used to anneal fibre ends. The left panel shows the heat gun used to heat fibre ends, the holding apparatus, and the electronics. The right panel shows the holding apparatus, the thermistor used for temperature measurements can be seen on the left side of the heat shield. Just below the thermistor is a hole into which the fibres were placed for heating.

95°C [67] and melting point of 240°C [68]. The temperature profile was manually followed for each annealing process to within ±10°C during the 120° phase, ±20°C during the melting phase, and to within ±60 s throughout the entire heating and cooling process.

During preliminary heating processes, before the holding apparatus was designed and built, it was noticed that fibres quickly expand in radius when heated. This led to the development of a heat shielding that protected the rest of the fibre from heat, so only the fibre-end was exposed. Also, because of the radial expansion, fibres needed to be inserted into a hole of the same radius to ensure fibres could not expand. Fortunately, the binding properties of PS and PMMA prevented the plastic

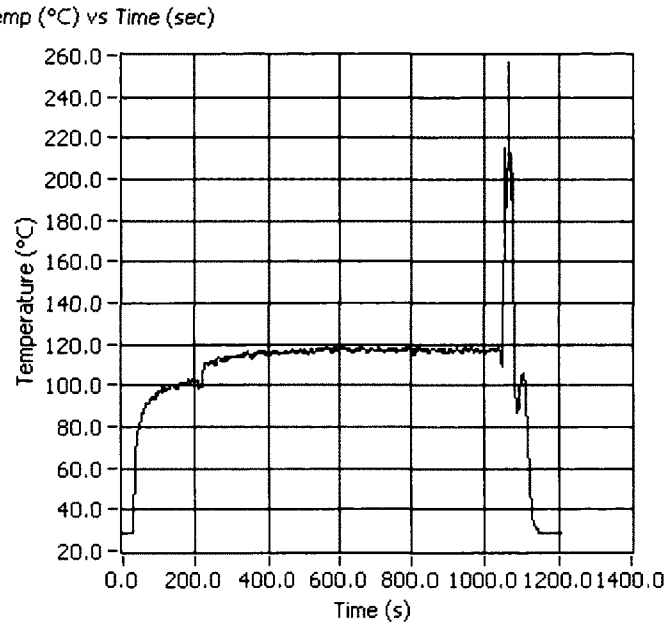

Figure 3.13: This temperature profile was followed to anneal fibre-ends through the annealing experiment. The fibre cores are made from PS which has glass transition temperature of 95°C [67] and a melting point of 240°C [68].

from binding to the securing metal hole, and thus was easily removed.

Temperature readings were collected using a thermistor probe [69] that was in a circuit wired to a DAQ card. The DAQ card was connected to a personal computer and the temperature profiles were generated using LabVIEW.

Because of budget and time limitations, not all fibre-end finishes could be prepared to be annealed; thus, only scissor cut and fine sandpaper (320 grit) were completed. Those two choices were made for two reasons:

1. A fine sandpaper finish was desired to see if annealing a sanded fibre-end would smooth it out. The annealed finish is shown in Figure 3.14, and when compared to Figure 3.8, it can be seen that annealing the fine sandpaper finish has only a

little smoothing effect. From the very low mean light transmission ratio using sanded fibre-ends (non-annealed) found during this experiment (shown later in Figure 3.16), this annealed fibre-end finish was not tested for light transmission.

2. Because of the simplicity and low cost of cutting fibres with scissors, a scissor cut finish was desired to be tested. The SEM image in Figure 3.11 shows that some fibres crack when cut, so this finish was not tested without annealing; but, it was possible (and hoped for) that the fibre would melt/bond back together with annealing. Hence, a scissor cut fibre-end finish was annealed for testing and is shown in Figure 3.15.

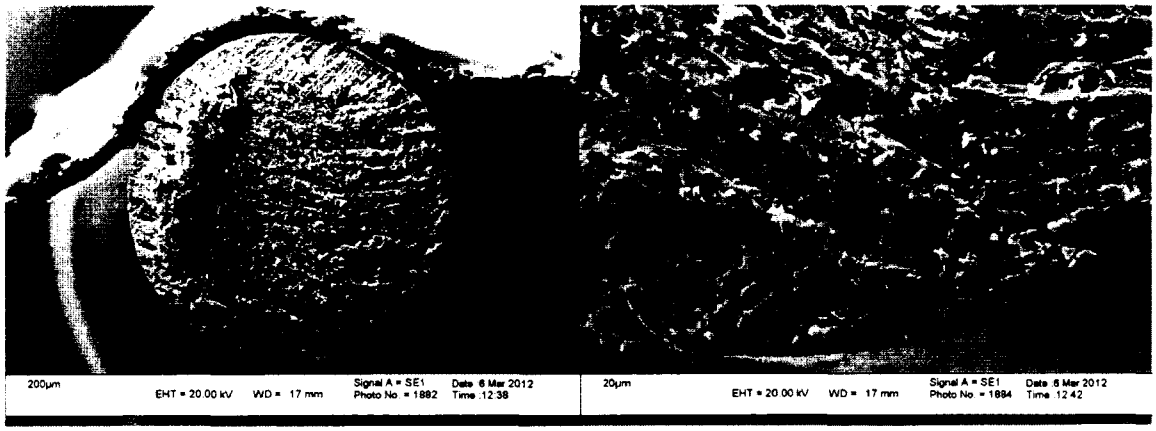

Figure 3.14: **Fine sandpaper/Annealed** - SEM photographs of a 320 grit finely sanded scintillating fibre-end that was annealed using the temperature profile in Figure 3.13. The left panel shows the full fibre-end. The right panel shows a zoomed in image of the same fibre. Note the PMMA cladding that circles around the edge of the fibre in panel. Image parameters are reported on the photograph.

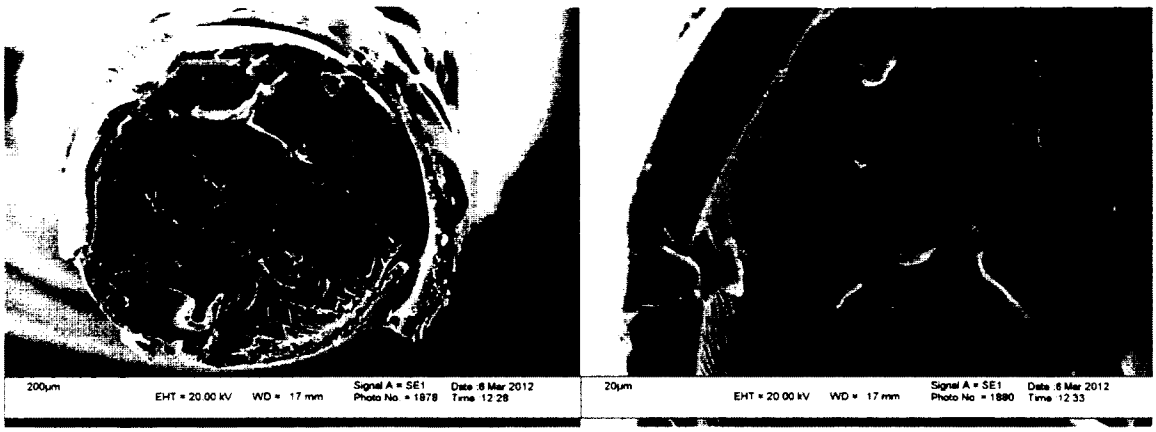

Figure 3.15: **Scissor Cut/Annealed** - SEM photographs of a scissor cut scintillating fibre-end that was annealed using the temperature profile in Figure 3.13. The left panel shows the full fibre-end. The right panel shows a zoomed in image of the same fibre. Note the PMMA cladding that circles around the edge of the fibre in panel. Image parameters are reported on the photograph.

From these SEM images, the smoother fibre-end finish which was scissor cut initially, was chosen to be tested with optical couplants. Once the scissor cut fibre-ends were annealed, couplants were then applied so that light transmission could be tested.

3.4 Application of Couplants

Only three types of optical couplants (air, optical grease, and optical epoxy) were used in these experiments since they were the most popular couplants previously used. The application process was very simple to ensure that a large scale project could easily adapt these methods.

Optical Grease: Light guides were inserted into the FCB and glued in place with 5 min epoxy. Once the epoxy was dried, finished scintillating fibres had a generous dab of 20-057 optical grease applied to their ends. The fibres were carefully inserted into the FCB's holes to ensure that the grease was not removed during insertion. If grease was removed, more was applied. Once scintillating fibres were touching light guide ends, they were rotated to provide a good connection between scintillating fibres ends and light guide ends. Scintillating fibres were then secured in place with epoxy. Since optical grease did not have to set, tests were performed once the securing epoxy was safely dried.

Optical Cement: EJ-500 Optical Cement was prepared according to the company's suggestion. Four parts resin were mixed with one part hardener by weight. Mixing formed small bubbles, which took for approximately one hour to come out of solution. The same procedure was then followed as above, but with optical cement rather then optical grease. Optical cement was given a minimum of 24 hours to dry before being disturbed for testing.

Air: The same light guide and scintillating fibre securing technique was used as above, but with no optical interface.

3.5 Data Collection and Analysis

Data was collected using PMT signals that were routed to an ADC module [59], which was read out by a Fortran program on a Unix-based computer. The program

was only responsible for collecting data and storing it in a format usable by a MATLAB program.

The MATLAB program was responsible for performing calculations for the final results and uncertainty analysis. Each data collection trial pertained to one FBC with one fibre-end finish type and one couplant type.

Data was entered into the analysis program in matrix format (D_{jk}) where D refers to the data, the subscript j refers to the fibre number and k is the event number. $j = 1, 2, 3$ were control fibres where $j = 4, 5, \ldots, 8$ were test fibres.

Test fibre values were normalized to the average of the control values on an event-by-event basis. This led to a ratio matrix (R_{ik}) where the subscript i is the normalized fibre number, and $i = 1, 2, \ldots, 5$ for the five test fibres. This ratio matrix then needed to be further the normalized to a calibration matrix (c_i) which contained "test fibre to control fibre" ratios for identical signal inputs (as discussed in Section 3.1.3).

Once R_{ik} was normalized to c_i, the values were fitted to a Gaussian curve. This gives rise to the equation:

$$\mu = \text{fit} \sum_{i=1}^{5} \sum_{k} \left(\frac{R_{ik}}{c_i} \right) \tag{3.1}$$

where μ is the mean light transmission ratio and the sum over k ran through all data points, typically around 6×10^5 for a 10 minute data-taking run. Each of the five test fibre holes had a placement uncertainty σ_{c_i} that reflects the uncertainty in position when securing the PCB to the PMT (as discussed in Section 3.1.3). σ_{c_i} was the main

source of uncertainty in this test. Applying Equation 2.6 to 3.1 gives:

$$\sigma_\mu^2 = \left(\frac{\bar{R}_1}{c_1^2}\sigma_{c_1}\right)^2 + \left(\frac{\bar{R}_2}{c_2^2}\sigma_{c_2}\right)^2 + \cdots + \left(\frac{\bar{R}_5}{c_5^2}\sigma_{c_5}\right)^2 + \sigma_{\text{fit}}^2 \tag{3.2}$$

Where $\bar{R}_i$ is the average test fibre-to-control fibre ratio for each fibre hole, and σ_μ is the uncertainty in μ.

Equations 3.1 and 3.3 were used to calculate the final values for $\mu \pm \sigma_\mu$, which were then compared graphically between different couplant and fibre-end finish combinations. Once fits and calculations were complete, the results were compared and conclusions were drawn.

3.6 Results

The results of this experiment were plotted using the fitted Gaussian distributions to easier visualize mean light transmission values and uncertainties. A comparison of the light transmission values with the optical couplants and fibre-end finishes was also made, and finally a ranking table to compare the different combinations.

Figure 3.16 is a collection of eight plots that has eight fit Gaussian distributions of the form:

$$f(x) = e^{\frac{-(\mu - x)^2}{2\sigma^2}} \tag{3.3}$$

where μ is the mean light transmission ratio for a fibre-end finish and optical couplant combination, and σ is the standard deviation of the distribution. For easier visualization, the fit Gaussian for each test-case's normalized light transmission ratio

has been scaled to have a peak value of unity. Because of this scaling to peak value of unity, it is possible to easily illustrate the location on all of the tests of the $\pm\sigma$ values of normalized light transmission using a horizontal line. The solid horizontal line at $f(x = \mu \pm \sigma) = 0.6065$ represents the $\pm\sigma$ line, and the dashed horizontal line at $f(x = \mu \pm \frac{\sqrt{2}}{2}\sigma) = 0.7788$ represents the $\pm\frac{\sqrt{2}}{2}\sigma$ line. The second line was used as a visual comparator to see if means were significantly different when subtracted from one another, where the uncertainties add in quadrature.

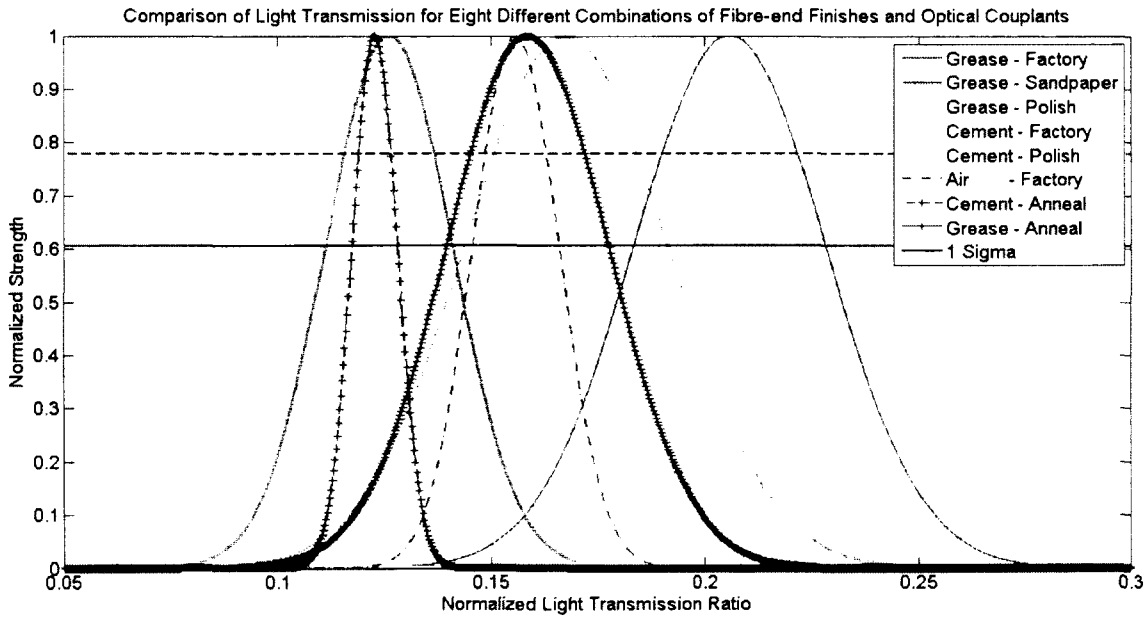

Figure 3.16: This figure compares the eight tested fibre-end finish and optical couplant combinations. The solid horizontal line represents the uncertainty in each measurement, while the dashed horizontal line is the line uncertainty when two different Gaussians are subtracted.

It can be seen from Figure 3.16 that the combination of grease/factory,

grease/polish and cement/polish have the highest light transmission ratio to within $\pm\sigma$. It can also be seen that grease/factory and grease/polish have a significantly higher light transmission ratio when compared to others by subtraction.

Table 3.1 shows the light transmission means and uncertainties with optical couplants and fibre-end finishes in columns and rows, respectively. The table is laid out for easy comparison between all different combinations. For example, it can be seen that for the optical grease couplant, factory finish and polish provides the highest light transmission ratios. Also, for the factory fibre-end finish, optical grease is the best couplant. Due to the cost of scintillating fibres and of machining all the required blocks, not all combinations of couplants and finishes were performed.

	Air ($\mu \pm \sigma_\mu$)	Grease ($\mu \pm \sigma_\mu$)	Cement ($\mu \pm \sigma_\mu$)
Factory	0.156 ± 0.010	0.206 ± 0.022	0.133 ± 0.023
Sandpaper	-	0.126 ± 0.015	-
Polish	-	0.197 ± 0.008	0.168 ± 0.024
Anneal*	-	0.159 ± 0.019	0.123 ± 0.005

Table 3.1: This table shows the light transmission means and uncertainties with optical couplants and fibre-end finishes in columns and rows respectively. * - Annealing was done after fibres were cut with fibre optic cutting scissors. Due to budget limitations, not all trials could be completed.

When comparing two mean transmission ratios, a difference can be taken to see if the values differ or are the same within uncertainty. This leads to the uncertainties adding in quadrature, which the dotted horizontal line in Figure 3.16 represents. In Table 3.2, each combination is considered with all others individually,

allowing a determination of which mean transmission ratio is higher, or if they are the same.

	G/F	G/S	G/P	G/A	C/F	C/P	C/A	Air/F
G/F	-	LT	Eq	LT	LT	LT	LT	LT
G/S	GT	-	GT	GT	Eq	GT	Eq	GT
G/P	Eq	LT	-	LT	LT	LT	LT	LT
G/A	GT	LT	GT	-	Eq	Eq	LT	Eq
C/F	GT	Eq	GT	Eq	-	GT	Eq	Eq
C/P	GT	LT	GT	Eq	LT	-	LT	Eq
C/A	GT	Eq	GT	GT	Eq	GT	-	GT
Air/F	GT	LT	GT	Eq	Eq	Eq	LT	-
+/-	+6	-5	+6	0	-3	+1	-5	0

Table 3.2: This table compares each different combination of optical couplants and fibre-end finishes relative to each other. Each comparison is made to the top of the column. For example, G/F is greater than G/S. The abbreviations refer to: GT - Greater Than; Eq - Equal; LT - Less Than. The "+/-" column puts a numerical value to the number of combinations a certain combination is better than. In the rows and colums the optical couplant is listed first (G - Optical Grease; C - Optical Cement; Air - Air) and the fibre-end finish is listed second (F - Factory Finish; S - Fine Sandpaper (320 grit); P - Polish; A - Annealed).

Table 3.2 shows the relative mean light transmission ratio strengths, indicating: (Grease/Factory = Grease/Polish) > Cement/Polish > (Grease/Anneal = Air/Factory) > Cement/Factory > (Grease/Fine Sandpaper (320 grit) = Cement/Anneal). These findings support that Grease/Factory and Grease/Polish are the best light transmitting combinations. Now that results have been shown and discussed, a concise conclusion can be stated.

Earlier in this thesis, it was cited that others had found a 98% transmission efficiency for optical grease [43], and 95% for optical epoxy [27], significantly higher than values reported in this thesis. It should be noted that the numbers reported in this thesis did not measure transmission efficiency of light at an interface, but rather the mean light transmission ratio using different fibre-end finishes in combination with different optical couplants. It was not the purpose of this thesis to measure the light transmission absolutely or directly, but to compare different combinations using the same measurement technique each time.

However, a reason for the reduction in light transmission compared to earlier reports is likely the following. The photocathode sensitivity of the H7546 PMT is wavelength dependent, providing a higher cathode radiant sensitivity for the blue light produced by the LED (468 nm maximum emission wavelength) compared to the green light released by the scintillating fibres (493 nm maximum emission wavelength). Also, the blue light sent down the scintillating fibres has a energy higher than the first electronic state of the π-electron structure. This may have allowed blue light corresponding to the first electronic state plus thermal states to be absorbed, and re-emitted isotropically as green light, causing a reduction in the fraction of initial blue light arriving at the PMT. These two points would have both caused a reduction in the normalized light transmission ratio, since the control light guides were unaffected by both points (because of not using the scintillating fibres), while the test fibres would have seen a reduced response.

3.7 Conclusion: Light Transmission

In conclusion for the light transmission experiment using different combinations of optical couplants and fibre-end finishes, the combination of optical grease with factory finish and optical grease with a polished finish have the highest light transmission, and are the same within experimental uncertainty.

A comparison of all optical couplant and fibre-end finish combinations, ranking from best to worst light transmission, is shown in Table 3.3. These results are consistent with Figure 3.16 in which the mean light transmission ratio and uncertainties are plotted at mean and standard deviations of Gaussian distributions.

	Couplant/Finish Combo.
Best Transmission	Grease/Factory and Grease/Polish
2nd	Cement/Polish
3rd	Grease/Anneal and Air/Factory
4th	Cement/Factory
Worst Transmission	Grease/Fine Sandpaper (320 grit) and Cement/Anneal

Table 3.3: This table compares each different combination of optical couplants and fibre-end finishes relative to each other, and orders them from best optical transmission to worst.

Another interesting result is that in every case, within the same fibre-end finish, optical grease provides a higher normalized light transmission ratio than optical epoxy/cement. This can be seen for every case where both grease and epoxy/cement were tested.

These results are in indirect agreement with two separate previous reports.

One paper found a 98% light transmission for optical grease [43], while another found a 95% light transmission for optical epoxy [27]. Additionally, these results are in indirect conflict with a previous report that found optical epoxy (cement) had a 15% higher light yield than optical grease [35]. However, those results are comparing the connection between light guides and a PMT photocathode, as opposed to the fibre-coupling compared here.

Chapter 4

Future Work

Throughout a literature review which has been reported in Chapter 1 of this thesis, a number of gaps in knowledge have been identified. These gaps will again be highlighted in this section.

The topic of connecting light guides to light collection devices was briefly discussed in Section 1.6.2, and not much literature was found on the topic. The field of experimental nuclear and particle physics could benefit from experiments to determine the best way to couple light guides and light collection devices together. More importantly, this topic seems very trivial and the outcome of such an experiment has most likely already been determined, but just not published explicitly.

With regard to reflective ends, as presented in Section 1.6.4, there was a conflict in the literature. The three common ways to coat fibre ends with reflective material should be tested thoroughly in one experiment that directly compare the light arriving at a light collection device after reflection.

The idea of using larger diameter light guides to collect scintillating fibre

light should be investigated. Although the literature review done for this thesis did not find any results, it is possible some exist. However, in the event that this has not been quantitatively investigated, knowing if using larger diameter light guides can increase light transmission would improve the construction of all future SFTs.

Appendix A

Experimental Parameters

A.1 Electronics Settings

Table A.1 includes important electronic settings on the NIM modules used in the "Effects of Fibre Coating on Adjacent Scintillating-to-scintillating Fibre Cross-talk" experiment.

A.2 Experimental Results

A comparison of experimental results collected from a literature review that was presented in Chapter 1 of this thesis is shown.

Fibre/Plate	Fan-out	Discriminator		
	t_{delay}	t_{delay}	$V_{thres.}$	ΔT_{width}
Uncertainty	±0.4 ns	±0.4 ns	±0.1 mV	±4
SF1	5.8	9.6	-15.0	50
SF2	4.2	9.4	-15.0	50
SF3	5.4	10.0	-15.0	50
SF4	5.4	9.6	-15.0	50
SF5	5.6	9.2	-15.0	50
SF6	5.6	8.8	-15.0	50
SF7	5.4	9.6	-15.0	50
SF8	5.6	9.6	-15.0	50
S1	-	-	-87.9	-
S2	-	-	-82.7	-

Fibre/Plate	Logic Unit			
	Inputs	Logic	t_{delay}	ΔT_{width}
Uncertainty	NA	NA	±0.4 ns	±4 ns
SF1 SF2 SF3 SF4	SF1-4 (c)	OR (1)	-	50
SF5 SF6 SF7 SF8	SF5-8 (c)	OR (1)	10	50
	SF1-4 & SF1-8 (d)	OR (1)	9.6	50
S1 S2	S1+S2 & SF1-8 (e)	AND (3)	9.6	50

Table A.1: Values of the Fan-out's input-to-output time delay t_{delay}; the Discriminator's input-to-output delay t_{delay}, threshold voltage $V_{thres.}$ and output pulse width ΔT_{width}; and the logic unit's inputs, boolean logic, input-to-output delay t_{delay} and output pulse width ΔT_{width}. The total delay for S1 and SF1 from the Fan-out output to the event trigger (Logic Unit (e)) output are 54.4±4 ns and 53.6±4 ns respectively, within uncertainty of each other. Under the Inputs sub-column in the Logic Unit column (c), (d) and (e) refer to the logic unit positions in Figure 2.3. The number after the type of boolean logic in the Logic sub-column indicates the required number of signals needed to achieve an output.

	DIRAC [35]	COMPASS [18, 35]	D0 Central Tracker [27]	ALFA [16]
LCD*	H6568 PMT	H6568 PMT	VLPC	R7600 PMT
Fibre Type	SCSF-38	SCSF-78MJ	(K)	SCSF-78
Diameter	0.5 mm	0.5 mm	0.835 mm	0.5
Coating	-	-	-	-
Column Pitch	0.43 mm	0.41 mm	-	-
Column Size	5	7	2	1
Layers	-	-	24 x 2	10
Reflector	Al.	Al. Mylar	Al. Mylar	1/2 w/ Al.
Multiplicity	1.1	1.035	-	-
Det. Eff. **	98%	98-99%	>99%	95%
Spatial Res.	125 μm	120 μm	136.2 μm	36μm
Time Res.	0.6 ns	0.36 ns	-	-

Table A.2: This table shows a summary of details discussed in the introduction section. A comparison between resolutions is not a good indicator of the quality of a tracker, since some trackers don't require high rates, or high precision. This data is compiled from all sources discussed. * is light collection device, ** is detection efficiency. H and R light collection devices are Hamamats made while. K and SCSF are Kuraray made.

Appendix B

Minimum Separation of Scintillating Plates

With reference to Figure 2.1, in order to be sure that one particle cannot pass through two scintillating fibres in sequence, the scintillating plates S1 and S2 must be separated a minimum distance h. A simplified schematic is shown in Figure B.1.

The largest angle a particle can achieve while passing though both scintillating plates S1, S2 and two scintillating fibres SF is by hitting one plate on the far right and the other on the far left. S1 and S2 are $w = 30$ mm wide, the fibre radius is $r = 0.5$ mm. It is assumed that a particle must pass through $d = 0.2$ mm of scintillating material before producing a detectable signal.

To determine the shallowest angle allowed before a particle passes through two the cosine law must be used:

$$b^2 = a^2 + c^2 - 2ac\cos\beta \tag{B.1}$$

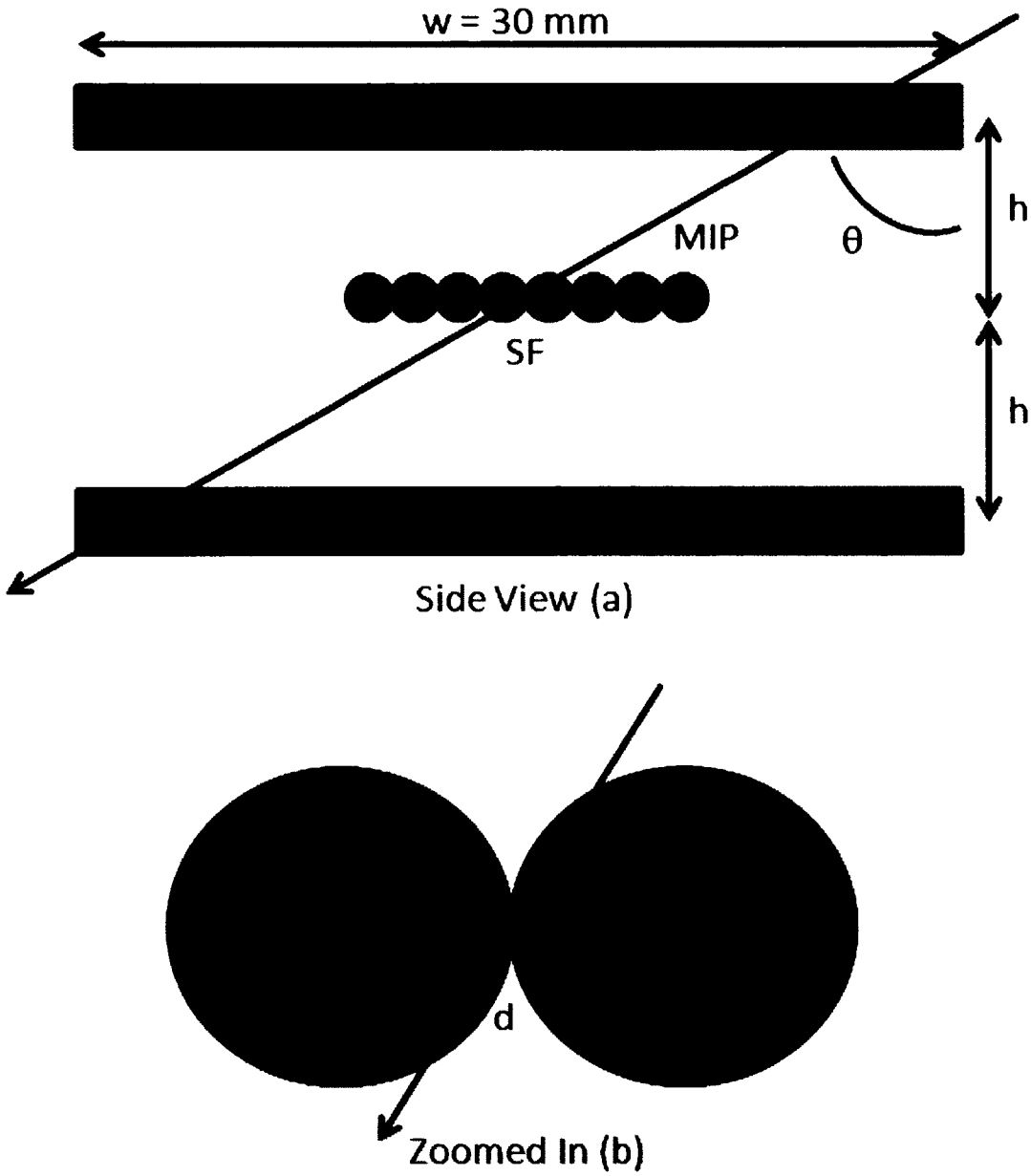

Figure B.1: In the side view (a), a MIP passes down through S1, S2 and two SFs. In the zoomed in view (b), the relation between the radius of the fibres $r = 0.5$ mm, the angle θ and the distance $d = 0.2$ mm a particle must pass through fibre in order to make a signal is shown.

where in this case $a, b = r$, $c = d$, and $\beta = \theta_{min}$. This reduces to:

$$\theta_{min} = \arccos\left(\frac{d}{2r}\right) = 78.4^{\circ} \tag{B.2}$$

This leads to $h = 73.48$ mm. If the plates were closer than this, one particle could pass through two scintillating fibres and appear as cross-talk. However, the effect was eliminated by separating plates to $h = 120$ mm.

Bibliography

[1] M. Atkinson, D. Crennell, C. Fisher, and N. Kurtz. Conceptual design for a high resolution high rate vertex detector for charm and beauty experiments using scintillating fibre optics. *Nuclear Instruments and Methods in Physics Research*, 225(1):1 – 7, 1984.

[2] L.R. Allemand, J. Calvet, J.C. Cavan, and J.C. Thévenin. Optical scintillating fibres for particle detectors. *Nuclear Instruments and Methods in Physics Research*, 225(3):522 – 524, 1984.

[3] W.R. Binns, J.J. Connell, P.F. Dowkontt, J.W. Epstein, M.H. Israel, and J. Klarmann. A scintillating optical fiber track imaging detector. *Nuclear Instruments and Methods in Physics Research Section A: Accelerators, Spectrometers, Detectors and Associated Equipment*, 251(2):402 – 406, 1986.

[4] M. Atkinson, J. Fent, C. Fisher, P. Freund, P. Hughes, J. Kirkby, A. Osthoff, and K. Pretzl. Initial tests of a high resolution scintillating fibre (scifi) tracker. *Nuclear Instruments and Methods in Physics Research Section A: Accelerators, Spectrometers, Detectors and Associated Equipment*, 254(3):500 – 514, 1987.

[5] Akira Konaka, Ken ichi Imai, Hajime Kobayashi, Akira Masaike, Kozo Miyake, Tadashi Nagamine, Tatsuro Nakamura, Noboru Sasao, and Yoshio Yoshimura. Plastic scintillating fibers for track detection. *Nuclear Instruments and Methods in Physics Research Section A: Accelerators, Spectrometers, Detectors and Associated Equipment*, 256(1):70 – 75, 1987.

[6] H. Blumenfeld, M. Bourdinaud, and J.C. Thevenin. Plastic fibers in high energy physics. *Nuclear Instruments and Methods in Physics Research Section A: Accelerators, Spectrometers, Detectors and Associated Equipment*, 257(3):603 – 606, 1987.

[7] H. Blumenfeld, M. Bourdinaud, H. Burmeister, R. Cester, P. Checchia, and G. Zumerle. An electromagnetic calorimeter prototype module using scintillating fibers immersed in a Bi-Pb alloy. *Nuclear Instruments and Methods in Physics Research*, 225(3):518 – 521, 1984.

[8] J. Ditta, K. Kuroda, A. Michalowicz, C. Nemoz, and D. Sillou. Test of a position sensitive photomultiplier hodoscope. *Nuclear Instruments and Methods in Physics Research Section A: Accelerators, Spectrometers, Detectors and Associated Equipment*, **240**(1):69 – 71, 1985.

[9] W. Brückner and M. Godbersen and Th. Kallakowsky and R. Michaels and S. Paul and B. Povh and K. Röhrich. A scintillating fibre hodoscope with avalanche photodiode readout. *Nuclear Instruments and Methods in Physics Research Section A*, **313**(3):429 – 436, 1992.

[10] M. Vander Donckt. Performances of the chorus scintillating fibre trackers. *Nuclear Physics B - Proceedings Supplements*, **54**(3):105 – 110, 1997.

[11] K. Morimoto et al. Scintillating Fiber Imager for RLGS. In *Nuclear Science Symposium, 1999. Conference Record. 1999 IEEE*, 1999.

[12] M. Leblanc, C. Raymond, H. Tricoire, and L. Valentin. SOFI: A Scintillating Optical Fiber Imager. *Nucl. Instr. and Meth. A*, 273(2-3):583 – 587, 1988.

[13] M. Bendali et al. Scintillating optical fiber detectors for dna sequencing. *Nucl. Instr. and Meth. A*, 310(1-2):373 – 378, 1991.

[14] H. Gast et al. A High Resolution Scintillating Fiber Tracker with SiPM Readout for the PEBS Experiment. *Nucl. Instr. and Meth. A*, 581:423–426, October 2007.

[15] S. Ask. Luminosity Measurement at ATLAS with a Scintillating Fiber Tracker. In *Nuclear Science Symposium Conference Record, 2006. IEEE*, nov 2006.

[16] S. Ask et al. Luminosity Measurement at ATLAS–Development, Construction and Test of Scintillating Fibre Prototype Detectors. *Nucl. Instr. and Meth. A*, 568(2):588 – 600, 2006.

[17] R.C. Chaney et al. Testing of the Spatial Resolution and Efficiency of Scintillating Fiber PET Modules. *IEEE, Trans. Nucl. Science*, 39:1472–1474, October 1992.

[18] S. Horikawa et al. A Scintillating Fiber Tracker With High Time Resolution for High-Rate Experiments. *IEEE, Trans. Nucl. Science*, 49(3):950, 2002.

[19] Stephen A. Dyer. *Wiley Survey of Instrumentation and Measurement.* Wiley-IEEE Press, 1st edition, 2001.

[20] Glenn F. Knoll. *Radiation Detection and Measurement.* John Wiley & Sons, Inc., 4th edition, 2010.

[21] William R. Leo. *Techniques for Nuclear and Particle Physics Experiments.* Springer-Verlag, 2nd edition, 1994.

[22] Richard C. Fernow. *Introduction to experimental particle physics*, chapter 1. Press Syndicate of the University of Cambridge, The Pitt Building, Trumpington St., Cambridge CB2 1RP, 1986.

[23] T. Yasuda et al. Measurement of Plastic Scintillating Fiber Properties with Avalanche Photodiodes. In *Nuclear Science Symposium and Medical Imaging Conference, 1991., Conference Record of the 1991 IEEE*, volume 1, pages 269 – 271, November 1991.

[24] R.F. Grazioso, R. Farrell, L. Cirignano, and K. Shah. APD arrays for Scintillating Fiber Readout. In *Nuclear Science Symposium, 1999. Conference Record. 1999 IEEE*, 1999.

[25] J.R. Macri et al. Readout of Scintillating Plastic Fibers with an APD Array and Prototype ASIC. *IEEE, Trans. Nucl. Science*, 50(4):928 – 935, 2003.

[26] B. Dolgoshein et al. Silicon Photomultiplier and its Possible Applications. *Nucl. Instr. and Meth. A*, 504(1-3):48 – 52, 2003.

[27] D. Adams et al. Performance of a Large Scale Scintillating fiber Tracker using VLPC Readout. *IEEE, Trans. Nucl. Science*, 42(4):401 – 406, August 1995.

[28] C. Zorn, F.J. Barbosa, A. Freyberger, and B. Kross. Scintillating Fiber-based Photon Beam Profiler for the Jefferson Lab Tagged Photon Beam Line. In *Nuclear Science Symposium Conference Record, 2000 IEEE*, 2000.

[29] A. Dyshkant et al. MAPMT H7546B Anode Current Response Study for an ILC SiD Muon System Prototype. *IEEE, Trans. Nucl. Science*, 55:1691–1694, June 2008.

[30] Branchini et al. Construction and Performance of a High Granularity Calorimeter. *IEEE, Trans. Nucl. Science*, 56(2):394 – 397, 2009.

[31] P. Achenbach et al. In-beam Tests of Scintillating Fibre Detectors at MAMI and at GSI. *Nucl. Instr. and Meth. A*, 593:353–360, August 2008.

[32] Hamamatsu, 314-5, Shimokanzo, Iwata City, Shizuoka Pref., 438-0193, Japan. *Multianode Photomultipler Tube Assembly - H7546B.* (URL: http://sales.hamamatsu.com/assets/pdf/parts_H/H7546A_H7546B_TPMH1240E12.pdf).

[33] C.F. Perdrisat et al. Particle Tracking with Scintillating Fibers and Position Sensitive Photomultipliers. In *Nuclear Science Symposium and Medical Imaging Conference, 1991., Conference Record of the 1991 IEEE*, volume 1, pages 331 – 335, November 1991.

[34] G. Roper Yearwood et al. A Scintillating Fiber Tracker With SiPM Readout. *Nucl. Phys. B - Proc. Suppl.*, 197(1):245–249, 2009. 11th Topical Seminar on Innovative Particle and Radiation Detectors (IPRD08).

[35] A. Gorin et al. Scintillating Fiber Hodoscopes for DIRAC and COMPASS experiments. *Czech. J. of Phys.*, 49:173 – 182, 1999.

[36] D. Nakajima et al. Scintillating fiber detectors for the HypHI project at GSI. *Nucl. Instr. and Meth. A*, 608(2):287 – 290, 2009.

[37] M.D. Petroff and M. Atac. High Energy Tracking Using Scintillating Fibers and Solid State Photomultipliers. *IEEE, Trans. Nucl. Science*, 36:163 – 164, 1989.

[38] M.J. Murray. The hermes recoil detector. In *Nuclear Science Symposium Conference Record, 2005 IEEE*, volume 2, pages 823 – 826, 2005.

[39] Y.S. Yoon et al. Design and Tests of the Scintillating Fiber Hodoscopes in the CREAM Instrument. In *29th International Cosmic Ray Conference Pune 2005*, volume 3, pages 433–436, 2005.

[40] M. Ellis *et al.* The design, construction and performance of the mice scintillating fibre trackers. *Nuclear Instruments and Methods in Physics Research Section A: Accelerators, Spectrometers, Detectors and Associated Equipment*, 659(1):136 – 153, 2011.

[41] U. *et al* Bravar. "design and testing of a position-sensitive plastic scintillator detector for fast neutron imaging". *Nuclear Science, IEEE Transactions on.* 53(6):3894 –3903, dec. 2006.

[42] Datema, C.P. and Meng, L.-J. and Ramsden, D. The Detection of Minimum Ionising Particles with Scintillating Fibres using Multi-pixel Hybrid Photodiodes. *IEEE, Trans. Nucl. Science*, 45(3):338 – 342, June 1998.

[43] M. Chung and S. Margulies. Development of a Multichannel Fiber-To-Fiber Optical Connector for the D0 Upgrade Tracker. *IEEE, Trans. Nucl. Science*, 43(3), June 1996.

[44] M. Salomon. New Measurements of Scintillating Fibers Coupled to Multianode Photomultipliers. *IEEE Trans. Nucl. Sci.*, 39:671–673, 1992.

[45] N. Mascarenhas, J. Lund, J. Peel, and D. Sunnarborg. Development of a Directional 14 MeV Neutron Detector using Scintillating Fibers. In *Nuclear Science Symposium Conference Record, 2005 IEEE*, volume 3, pages 1515 –1518, 2005.

[46] R.M. Kippen et al. Simulations and Preliminary Results from the SIFTER (Scintillating Fiber Telescope for Energetic Radiation) Beam Test Apparatus. In *Nuclear Science Symposium, 1998. Conference Record. 1998 IEEE*, 1998.

[47] S. Aota et al. Development of Fiber-to-fiber Connectors for Scintillating Tile/fibre Calorimeters. *Nuclear Instruments and Methods in Physics Research A*, 357:71 – 77, 1995.

[48] Kuraray America Inc., 200 Park Avenue, NY 10166, USA.

[49] Saint-Gobain Crystals, Paris, France. (URL: http://www.bicron.com).

[50] Bicron Corporation, 12345 Kinsman Road, Newbury, OH 44065.

[51] A.G. Weisenberger et al. Application of Small Inexpensive Side-on (Side-window) Photomultiplier Tubes for Scintillating Fiber Readout. In *Nuclear Science Symposium and Medical Imaging Conference, 1991., Conference Record of the 1991 IEEE*, volume 1, pages 336 – 340, November 1991.

[52] S. Margulies. Effects of Hadron Irradiation on Scintillating Fibers. In *Nuclear Science Symposium and Medical Imaging Conference, 1992., Conference Record of the 1992 IEEE*, volume 2, pages 810 – 812, October 1992.

[53] K.G. Young et al. Effects of Radiation on Scintillating Fiber Performance. In *Nuclear Science Symposium and Medical Imaging Conference, 1992., Conference Record of the 1992 IEEE*, volume 2, pages 804 – 806, October 1992.

[54] J.S. Legere et al. A High Fidelity Scintillating Fiber Tracker for SONTRAC. In *Nuclear Science Symposium Conference Record, 2006. IEEE*, volume 1, pages 417 – 420, November 2006.

[55] Matsusada Precision Inc., 80 Orville Drive, Suite 100, Bohemia, NY 11716, USA. *JB-1.5N High Voltage Power Supply* . (URL: http://www.matsusada.com/pdf/JB.pdf).

[56] Burle Industries, Inc., Tube Products Division, 1000 New Holland Ave., Lancaster, PA 17601-5688 US. *Burle 8575 Photomultiplier Tube.* (URL: https://mipp-docdb.fnal.gov:440/cgi-bin/RetrieveFile?docid=281;filename=8575.pdf;version=1).

[57] Phillips Scientific, 31 Industrial Ave., Mahwah, NJ 07430, USA. *NIM Model 748 - Octal Linear/Logic Fan-Out.* (URL: http://www.phillipsscientific.com/pdf/748ds.pdf).

[58] Phillips Scientific, 31 Industrial Ave., Mahwah, NJ 07430, USA. *NIM Model 710 - Octal Discriminator.* (URL: http://www.phillipsscientific.com/pdf/710ds.pdf).

[59] Lecroy, 700 Chestnut Ridge Rd., Chestnut Ridge, NY 10977, USA. *CAMAC Model 2249A 12 Channel A-to-D Converter.* (URL: http://www.lecroy.com/lrs/dsheets/2249.htm).

[60] Phillips Scientific, 31 Industrial Ave., Mahwah, NJ 07430, USA. *NIM Model 756 - Quad Majority Logic Unit.* (URL: http://www.phillipsscientific.com/pdf/756ds.pdf).

[61] Kinetic Systems, 700 Chestnut Ridge Rd., Chestnut Ridge, NY 10977, USA. *3610 Hex Scalar.*

[62] A.H. Wapstra and G. Audi. The 1983 atomic mass evaluation: (I). Atomic mass table. *Nuclear Physics A*, 432(1):1 – 54, 1985.

[63] BK Precision Corporation, 22820 Savi Ranch Parkway, Yorba Linda, CA 92887-4610, USA. *Model 2540 Oscilloscope.* (URL: https://www.valuetronics.com/Manuals/BK_2534_2540_2542.pdf).

[64] John R. Taylor. *An Introduction to Error Analysis.* University Science Books, 2nd edition, 1997.

[65] Philip R. Bevington and D. Keith Robinson. *Data Reduction and Error Analysis for the Physical Sciences.* McGraw-Hill, Inc., 2nd edition, 1992.

[66] Berkeley Nucleonics, 2955 Kerner Blvd., San Rafael CA 94901 USA. *BNC Model 8010 Pulse Generator.* (URL: http://www.berkeleynucleonics.com/products/model-8010.html#).

[67] Charles E. Wilkes. *PVC Handbook.* Hanser Gardner Publications Inc., 6915 Valley Avenue, Cincinnati, Ohio 45244-3029, USA, 1st edition, 2005.

[68] International Programme on Chemical Safety - INCHEM. *Polystyrene.* (URL: http://www.inchem.org/documents/icsc/icsc/eics1043.htm).

[69] Honeywell Sensing and Control. *1kω NTC - 120 Series Mini Thermistor Probe.* (URL: http://search.digikey.com/ca/en/products/120-102EAJ-Q01/480-3119-ND/1886005).